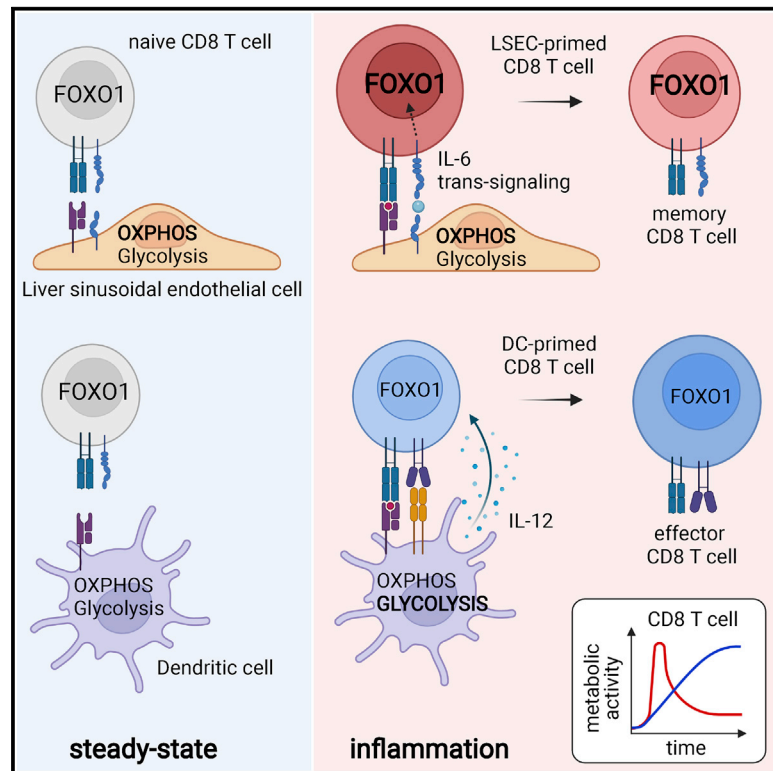


IL-6-induced FOXO1 activity determines the dynamics of metabolism in CD8 T cells cross-primed by liver sinusoidal endothelial cells

Graphical abstract



Authors

Michael Dudek, Kerstin Lohr, Sainitin Donakonda, ..., Stefan Rose-John, Hans Zischka, Percy A. Knolle

Correspondence

percy.knolle@tum.de

In brief

Dudek et al. find that liver sinusoidal endothelial cells (LSECs) with high mitochondrial respiration and low glycolysis facilitate regulatory immune functions despite inflammatory signaling. CD8 T cell activation through LSECs is dictated by IL-6 trans-signaling achieving FOXO1-dependent transient metabolic activity, revealing metabolic characteristics of local hepatic T cell activation.

Highlights

- Metabolic profile of LSECs of low glycolytic and high mitochondrial activity
- Lack of glycolytic switch and functional maturation in LSECs after activation
- Transient increase of immunometabolic activity in LSEC-primed CD8 T cells
- IL-6 signaling and FOXO1 in LSEC-primed CD8 T cells regulate immunometabolism



Article

IL-6-induced FOXO1 activity determines the dynamics of metabolism in CD8 T cells cross-primed by liver sinusoidal endothelial cells

Michael Dudek,^{1,10} Kerstin Lohr,^{1,10} Sainitin Donakonda,¹ Tobias Baumann,¹ Max Lüdemann,¹ Silke Hegenbarth,¹ Lena Dübbel,¹ Carola Eberhagen,² Savvoula Michailidou,¹ Abdallah Yassin,¹ Marco Prinz,^{3,4,5} Bastian Popper,⁶ Stefan Rose-John,⁷ Hans Zischka,^{2,8} and Percy A. Knolle^{1,9,11,*}

¹Institute of Molecular Immunology and Experimental Oncology, University Hospital München rechts der Isar, Technical University of Munich, Ismaningerstr. 22, 81675 München Germany

²Institute of Toxicology, Helmholtz Center München, München, Germany

³Institute of Neuropathology, Faculty of Medicine, University of Freiburg, Freiburg im Breisgau, Germany

⁴Center for NeuroModulation, Faculty of Medicine, University of Freiburg, Freiburg im Breisgau, Germany

⁵Signalling Research Centres BIOSS and CIBSS, University of Freiburg, Freiburg im Breisgau, Germany

⁶Biomedical Center, Ludwig-Maximilians-University Munich, München, Germany

⁷Institute of Biochemistry, University of Kiel, Kiel, Germany

⁸Institute of Toxicology and Environmental Hygiene, Technical University Munich, München, Germany

⁹German Center for Infection Research, Munich site, München, Germany

¹⁰These authors contributed equally

¹¹Lead contact

*Correspondence: percy.knolle@tum.de

<https://doi.org/10.1016/j.celrep.2022.110389>

SUMMARY

Liver sinusoidal endothelial cells (LSECs) are liver-resident antigen (cross)-presenting cells that generate memory CD8 T cells, but metabolic properties of LSECs and LSEC-primed CD8 T cells remain understudied. Here, we report that high-level mitochondrial respiration and constitutive low-level glycolysis support LSEC scavenger and sentinel functions. LSECs fail to increase glycolysis and co-stimulation after TLR4 activation, indicating absence of metabolic and functional maturation compared with immunogenic dendritic cells. LSEC-primed CD8 T cells show a transient burst of oxidative phosphorylation and glycolysis. Mechanistically, co-stimulatory IL-6 signaling ensures high FOXO1 expression in LSEC-primed CD8 T cells, curtails metabolic activity associated with T cell activation, and is indispensable for T cell functionality after re-activation. Thus, distinct immunometabolic features characterize non-immunogenic LSECs compared with immunogenic dendritic cells and LSEC-primed CD8 T cells with memory features compared with effector CD8 T cells. This reveals local features of metabolism and function of T cells in the liver.

INTRODUCTION

Cellular metabolism in professional antigen-presenting cells, such as dendritic cells (DCs), is closely linked to their function to activate adaptive immunity (Ganeshan and Chawla, 2014; Pearce et al., 2013). During steady-state non-inflammatory situations, prototypic professional antigen-presenting cells like DCs, as well as resting T cells, preferentially employ mitochondrial oxidative phosphorylation (OXPHOS) to fuel cellular functions and sustain longevity (O'Neill and Hardie, 2013). However, when DCs are activated by signaling through immune sensory receptors like Toll-like receptors (TLRs) or cytokines, or when T cells are activated by signaling through the T cell receptor and co-stimulatory receptors, such activated immune cells increase their glycolytic activity (Buck et al., 2017; Fox et al., 2005; Frauwirth et al., 2002). The increase in glycolysis is key to inducing immunogenicity of DCs and cytotoxic capacity of

CD8 T cells (Everts et al., 2014). This change in cell metabolism ensures the generation of bioenergetic building blocks and ATP molecules to supply cellular energy necessary for cytokine release, proliferation, and execution of T cell effector functions (Buck et al., 2017; Chang et al., 2013; Everts et al., 2014; Pearce et al., 2013).

The liver serves a dual function as a metabolic and immunological organ. It receives, via portal venous blood, nutrients from the gastrointestinal tract as well as pro-inflammatory TLR ligands derived from gastrointestinal microbiota (Balmer et al., 2014; Rui, 2014). Notwithstanding the abundance of nutrients and constitutive presence of pro-inflammatory stimuli, the hepatic immune milieu is dominated by induction of immune tolerance rather than immunity (Crispe, 2014; Thomson and Knolle, 2010). Beyond paracrine regulation of T cell immunity through regulatory immune cell populations and lack of immunogenic interleukin (IL)-12 production in the liver (Pallett et al., 2015;



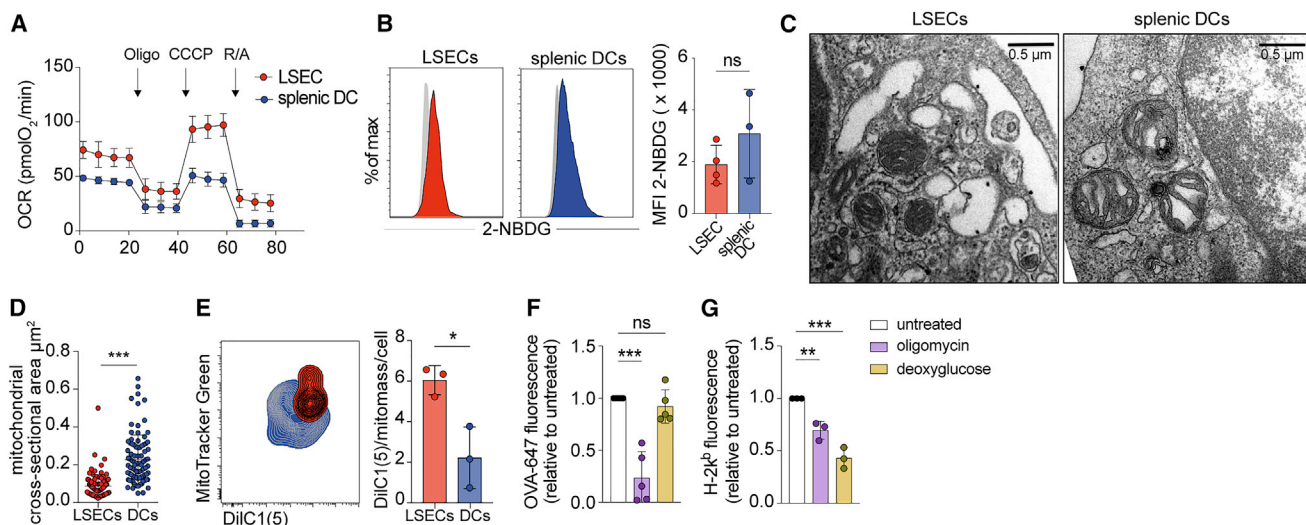


Figure 1. High-level mitochondrial oxidative phosphorylation in LSECs

(A) Representative profiles of oxygen consumption rate (OCR) measured by extracellular flux analysis in LSECs compared with DCs. (B) Flow cytometric analysis of glucose (2-NBDG) uptake by LSECs (n = 4) and splenic DCs (n = 3). (C) Ultrastructural analysis of mitochondria in LSECs and splenic DCs by transmission electron microscopy shown in representative images. (D) Quantification of ≥ 100 cross-sectional areas of mitochondria per group (from [C]), scale bars 0.5 μm. (E) Overlay plot of MitoTracker Green and DiIC1(5) fluorescence intensity detected by flow cytometry in LSECs or DCs (n = 3). Mitochondrial membrane potential in relation to mitochondrial mass per cell was calculated as ratio of mean fluorescence intensity of DiIC1(5) to that of MitoTracker Green. (F and G) Influence of deoxyglucose or oligomycin on LSEC scavenger activity of ovalbumin-647 uptake (OVA-647) (n = 5) and on surface expression of H-2K^b determined by flow cytometric measurement (n = 3). Data are representative of at least three separate experiments. ns, not significant; MFI, mean fluorescence intensity. One-way ANOVA with Tukey's multiple comparison test (F and G) and unpaired two-tailed t test (B, D, and E). In (A, B, and D–G), data are mean ± SEM and errors are shown as SD.

Schurich et al., 2013), liver-resident antigen-presenting cells, in particular liver sinusoidal endothelial cells (LSECs), contribute to local induction of T cell tolerance (Böttcher et al., 2013; Carambia et al., 2015; Diehl et al., 2008; Limmer et al., 2000). LSEC-primed CD8 T cells develop memory-cell-like features and migrate to adjacent lymph nodes, show long-term survival, and can differentiate into effector T cells under inflammatory conditions, similar to central-memory T cell (Böttcher et al., 2013). In contrast, tolerogenic DCs that lack co-stimulatory molecules induce T cell deletion, anergy, or polarization toward a regulatory phenotype (Horton et al., 2017). The metabolic demands for the tolerogenic functions of DCs are mainly covered by fatty acid oxidation (FAO)-dependent OXPHOS activated by peroxisome proliferator-activated receptor (PPAR)-γ signaling (O'Neill and Pearce, 2016). However, the metabolic requirements of tolerogenic LSECs and LSEC-primed memory CD8 T cells that support hepatic immune tolerance are unknown.

Here, we report that the metabolic phenotype of liver-resident LSECs is characterized by high-level mitochondrial OXPHOS and constitutive low-level glycolysis, which are instrumental in supporting their immune functions as scavenging and antigen-cross-presenting cells, but fail to undergo functional maturation and increase their glycolytic activity after TLR4 stimulation. CD8 T cells cross-primed by LSECs showed an IL-6-induced FOXO1-dependent shutdown of initial high metabolic activity that allowed for development of memory T cell functions, such as production of cytokines and sustained proliferation after antigen re-encounter.

RESULTS

Constitutive highly active mitochondrial respiration but low glycolytic activity in LSECs

We first characterized the metabolism of LSECs under steady-state conditions by extracellular flux analysis and compared it with the metabolic profile of freshly isolated splenic DCs. LSECs showed a higher level of OXPHOS compared with splenic DCs, as determined by elevated basal oxygen consumption, ATP production, maximal respiration, and spare respiratory capacity (Figures 1A and S1A). In contrast, we only detected minimal glycolytic activity and glucose uptake in LSECs either directly after isolation or after 48 h of *in vitro* culture (Figures 1B, S1B, and S1C). Because high-level mitochondrial respiration has been linked to a tight cristae structure in mitochondria (Klein Geltink et al., 2017), we investigated the mitochondrial ultrastructure in LSECs after isolation *in vitro* as well as *in situ* in liver tissue. LSECs cultured *in vitro* showed tight mitochondrial cristae as revealed by transmission electron microscopy (Figure 1C), with the mean diameter of mitochondria in LSECs being significantly smaller than that in DCs (Figure 1D). Using perfusion-fixed liver tissue for ultrastructural analysis by transmission electron microscopy, we confirmed tight cristae structure of mitochondria in LSECs also *in situ* (Figure S1D). We further identified a high mitochondrial membrane potential, which is instrumental to drive the mitochondrial electron transport chain for ATP generation (Lieberman et al., 1969), in LSECs compared with splenic DCs using the potentiometric mitochondrial dye (DiIC1[5]), which confirmed

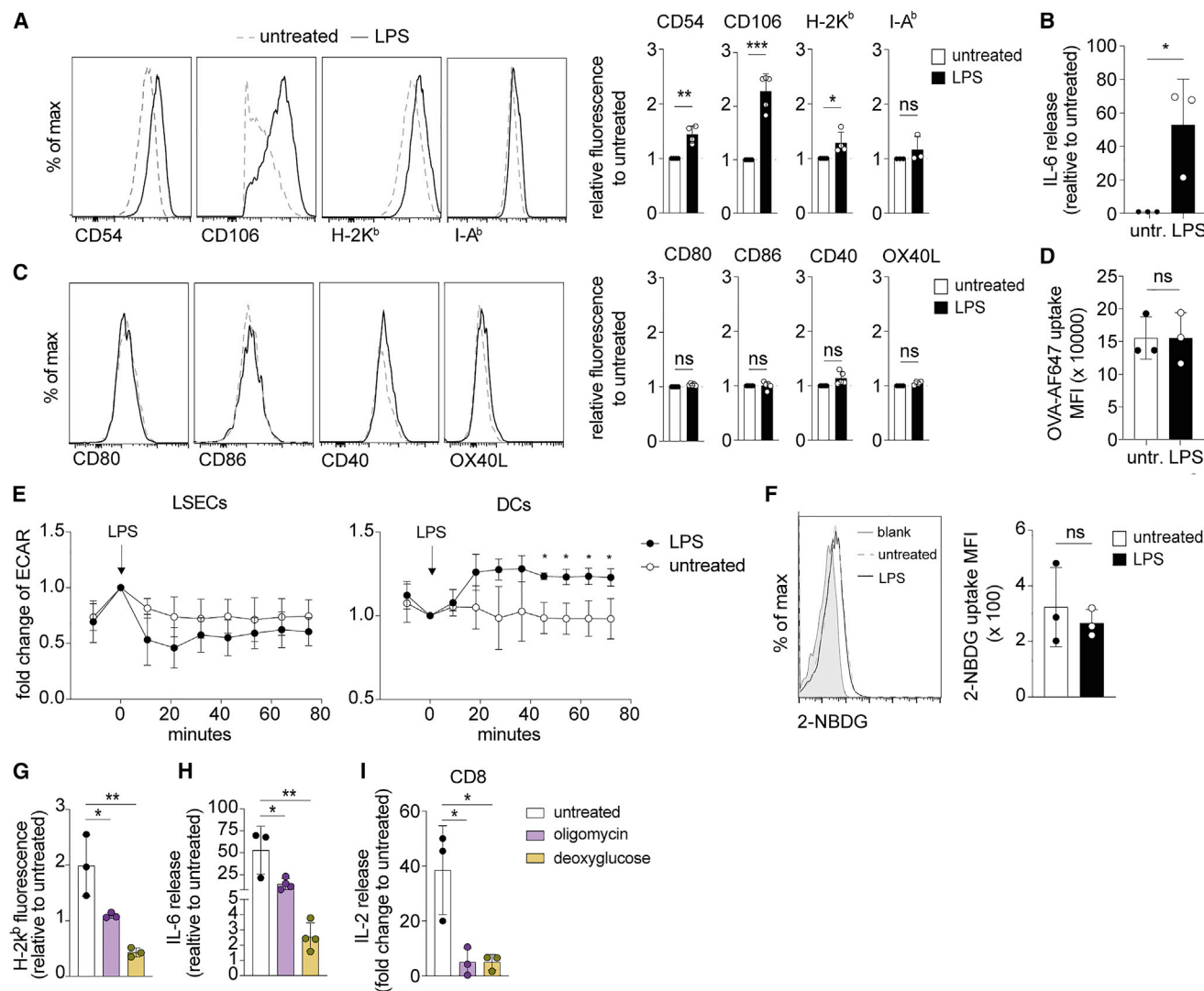


Figure 2. LSECs fail to respond to TLR4 activation with increased glycolytic activity or expression of co-stimulatory molecules

(A–D) LSECs were stimulated with LPSs *in vitro* for 18 h, and cell activation was measured by detection of increased expression of surface molecules (A, C), ELISA for IL-6 production (B), or scavenger activity (D). (A, C) Surface expression levels of CD54, CD106, H-2K^b, and I-A^b (A) and of CD80, CD86, CD40, and OX40L (C) and quantification as fold-change compared with untreated LSECs (n = 4). IL-6 release (B) from LSECs (n = 3) and OVA-647 uptake (D) in LSECs in absence or presence of LPSs (n = 3).

(E) Time kinetics of glycolysis in LSECs measured as extracellular acidification rate (ECAR) and splenic DCs after LPS challenge in supernatants (n = 3).

(F) Glucose uptake by LSECs after TLR4 stimulation (n = 3).

(G and H) LSEC H-2K^b expression (n = 3) (G) and IL-6 release (n = 4) (H) after TLR-4 stimulation in absence or presence of deoxyglucose or oligomycin.

(I) IL-2 release from ovalbumin-specific H-2K^b-restricted CD8 T cells activated by LSECs cross-presenting ovalbumin-derived peptides (S8L), previously exposed to deoxyglucose or oligomycin (n = 3).

Data are representative of at least two separate experiments. ns, not significant; MFI, mean fluorescence intensity. One-way ANOVA with Dunnett's multiple comparison test (G–I) and unpaired two-tailed t test (A–D and F). In (A–D and F–I), data are mean ± SEM; errors are shown as SD.

high OXPHOS rates (Figure 1E). Interestingly, high mitochondrial respiration in LSECs was not fueled by one particular energy substrate, because the uptake of different metabolites or pharmacological inhibition of mitochondrial uptake of distinct metabolites, such as pyruvate, fatty acids (FAs), or glutamate, did not affect the oxygen consumption rate (Figures S1E and S1F). This suggested that LSECs employed diverse nutrient sources for mitochondrial respiration.

Next, we investigated whether the metabolic profile and associated signaling pathways supported the immune functions of LSECs. We reasoned that the extraordinary scavenger activity of LSECs to endocytose soluble molecules through rapid receptor-mediated endocytosis (Sorensen et al., 2012) required high energy supply and therefore depended on mitochondrial respiration. Indeed, selective inhibition of mitochondrial ATPase but not of glycolysis prevented more than 90% of the rapid uptake of

fluorochrome-labeled ovalbumin and acetylated low-density lipoprotein in LSECs irrespective of the time after isolation (Figures 1F, S1G, and S1H). Thus, high-level mitochondrial respiration in LSECs fueled their energy-demanding scavenger function. Of note, expression of H-2K^b molecules and CD54, relevant for adhesion and major histocompatibility complex (MHC)-restricted cognate interaction with T cells, depended on both mitochondrial respiration and glycolysis under steady-state conditions (Figures 1G and S1I). We sought to narrow down the pathways in LSECs that controlled immune functions. Treatment of LSECs with pharmacological inhibitors of FOXO1 or NOTCH1 signaling, both relevant for vascular development in endothelial cells (Wilhelm et al., 2016), affected neither scavenger function nor glucose uptake. Interleukin-1 (ICAM)-1 expression, however, that is a target gene of FOXO1, was downregulated by FOXO1 inhibition (Figure S1J), indicating a distinct role for FOXO1 in microvascular LSECs compared with macrovascular endothelial cells (Andrade et al., 2021; Wilhelm et al., 2016). Together, these results indicate that constitutive high-level mitochondrial respiration in LSECs was associated with tight mitochondrial cristae structure and supported effective scavenging functions, which were independent of FOXO1 and NOTCH1 signaling.

Low glycolytic activity in LSECs is involved in response to TLR4 activation for IL-6 release but not for expression of co-stimulatory molecules

We next addressed the question of which consequences cellular metabolism had for immune functions in LSECs under inflammatory conditions, i.e. after TLR4 stimulation. Upon challenge with the TLR4 ligand lipopolysaccharides (LPSs), LSECs increased surface expression levels of CD54, CD106, and MHC class I molecule H-2K^b and released high amounts of IL-6 (Figures 2A and 2B). Strikingly, surface expression of MHC class II molecule I-A^b or of co-stimulatory molecules like CD80, CD86, CD40, and OX40L or gene expression of IL-12p35 remained unaffected in LSECs (Figures 2C and S2A), whereas surface expression levels of CD40 and CD86 and mRNA levels of IL-12p35 were upregulated by splenic DCs upon TLR4 stimulation (Figures 2C, S2A, and S2B). Of note, scavenging activity of LSECs was not increased upon LPS stimulation (Figure 2D). Importantly, LSECs failed to enhance glycolysis after TLR4 stimulation (Figures 2E and 2F), consistent with their non-immunogenic functions. Enforcing glycolysis through pharmacological activation of mTOR (mammalian target of rapamycin) was ineffective in LSECs, indicating a cell-intrinsic restriction of glycolysis (Figure S2C). Because enhanced glycolytic activity after TLR4 stimulation is necessary for DCs to become immunogenic, we wondered whether the restriction in glycolytic activity in LSECs after TLR4 stimulation affected the dynamics of H-2K^b/CD54 and IL-6 expression. Indeed, the constitutive low glycolytic activity in LSECs was required for the increase in H-2K^b/CD54 and IL-6 expression after TLR4 stimulation, because pre-treatment of LSECs with deoxyglucose as an inhibitor of glycolysis completely prevented LPS-induced increase in expression of these molecules (Figures 2G, 2H, S2D, and S2E). Strikingly, the capacity of LSECs to serve as antigen-cross-presenting cells was lost after treatment with oligomycin or deoxyglucose,

because after either treatment of LSECs, CD8 T cells failed to release IL-2 or express granzyme B (GzmB) (Figures 2I and S2F). This indicated that both OXPHOS and glycolysis were required for LSECs to cross-present soluble antigens on H-2K^b molecules to CD8 T cells. Furthermore, these results suggested that high mitochondrial respiration was critical for the energy-demanding process of antigen scavenging and that the consistently low glycolytic activity sufficed for LPS-dependent increase of H-2K^b expression and IL-6 secretion. Together, these results demonstrated a fundamental difference between splenic DCs and LSECs that failed to increase their glycolytic activity after TLR4 stimulation to become immunogenic antigen-presenting cells.

Cross-priming LSECs instruct unique dynamics of metabolism in CD8 T cells

It is well established that immunogenic DCs re-program CD8 T cell metabolism toward high glycolytic activity, leading to effector CD8 T cell differentiation, whereas immature DCs promote development of anergic or regulatory T cells (O'Neill and Pearce, 2016). We therefore set out to determine whether cross-priming LSECs shaped the metabolic program of CD8 T cells. Naive OT1 CD8 T cells bearing a transgenic T cell receptor specific for the ovalbumin-derived peptide SIINFEKL (S8L) were co-cultured with either ovalbumin-loaded and LPS-treated LSECs or splenic DCs for 24 or 72 h, and their metabolic profiles were analyzed. Unexpectedly, LSEC-primed CD8 T cells showed a rapid oxidative and glycolytic burst within 24 h that was followed by a decline in OXPHOS and glycolytic activity at 72 h after activation (Figures 3A–3F and S3A–S3D). In contrast, the glycolytic activity and mitochondrial respiration of DC-primed CD8 T cells increased from 24 to 72 h after activation (Figures 3A–3F, S3A–S3D). Consistent with the distinct dynamics of glycolysis of LSEC-primed CD8 T cells measured by metabolic flux analyses, gene expression levels of key enzymes for glycolysis and glucose uptake in LSEC-primed CD8 T cells were high at 24 h compared with in DC-primed CD8 T cells at 72 h (Figures 3G and S3E). Furthermore, expression of the activation markers CD25 and CD44 in LSEC- and DC-primed CD8 T cells paralleled the dynamics of T cell metabolism (Figures 3H, S3F, and 3G). To further characterize the relevance of antigen uptake by LSECs *in vivo* for cross-priming of CD8 T cells, we isolated LSECs and splenic DCs from mice 1 h after intravenous injection of ovalbumin. Only OT-1 CD8 T cells cultured with LSECs from ovalbumin-injected mice, but not splenic DCs or LSECs from untreated mice, showed a rapid increase in glycolysis and an increased expression of activation markers (Figures 3I and S3G).

We next characterized the metabolic profile of LSEC-primed CD8 T cells in more detail, focusing on FAO. Surprisingly, LSEC-primed CD8 T cells only utilized exogenous but not endogenous FAs to generate ATP (Figure S3H). Similar expression levels of key enzymes of FAO, i.e., *Cpt1a* and *Atgl*, confirmed results from metabolic flux analysis in LSEC-primed CD8 T cells (Figure S3I), suggesting use of exogenous FAs in addition to glucose as substrate source for generation of ATP, which resembles a metabolic feature of T_{rm} (tissue-resident memory T cells) (Pan and Kupper, 2018). This prompted us to

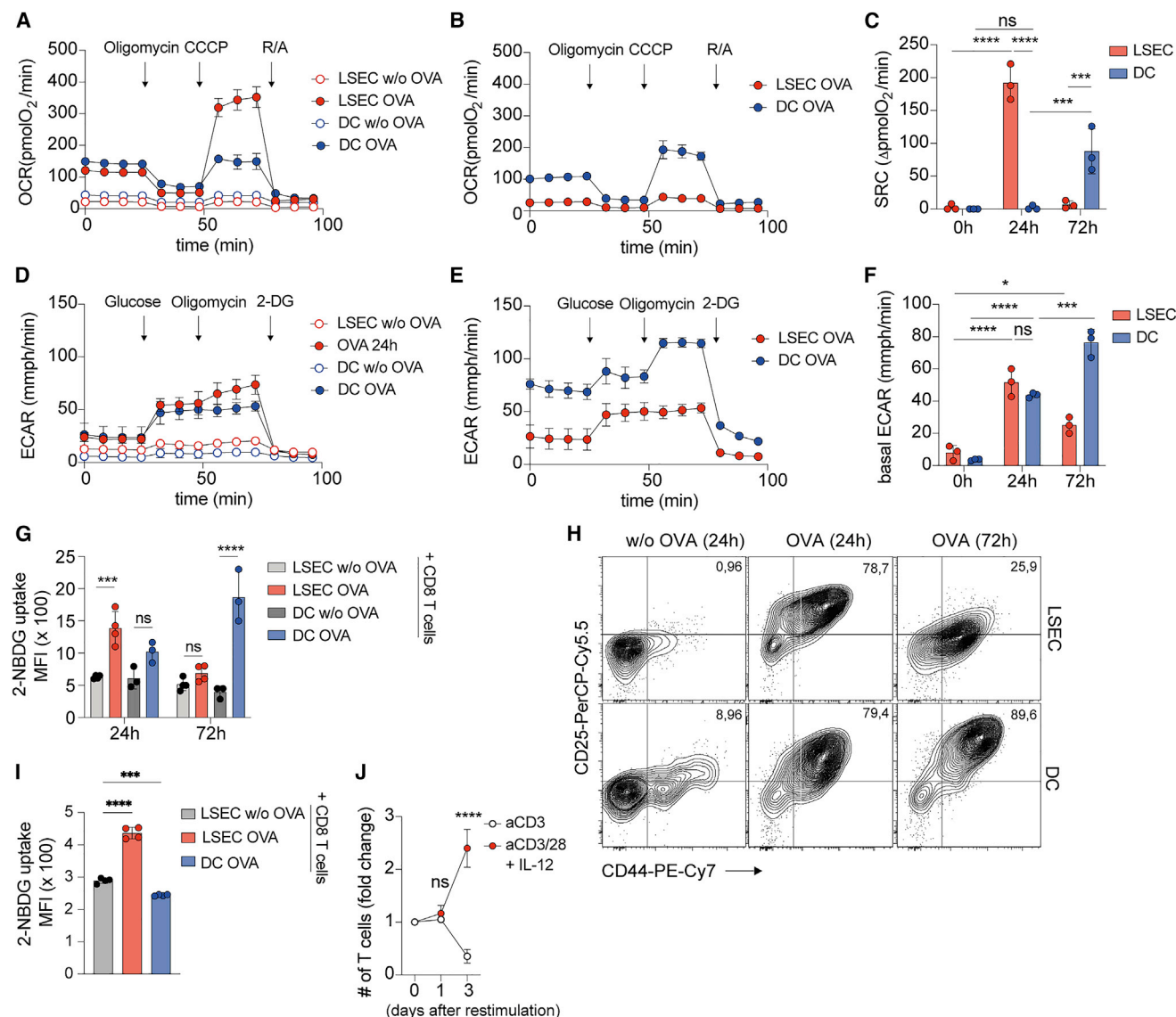


Figure 3. Metabolic profile of LSEC-primed CD8 T cells is characterized by high initial activity of glycolysis and mitochondrial respiration
(A–F) Representative profiles of oxygen consumption rate (OCR) during mitochondrial stress test and extracellular acidification rate (ECAR) during glucose stress test measured by extracellular flux analysis in SIINFEKL-specific OT1 CD8 T cells after 24 and 72 h after priming by LSECs or DCs. OCR and ECAR were quantified and SRC (C) and basal ECAR (F) were calculated (n = 3).
(G) Flow cytometric analysis of 2-NBDG, a fluorescently labeled glucose analogue, to measure glucose uptake in SIINFEKL-specific OT1 CD8 T cells at single cell level at 24 and 72 h after cross-priming by LSECs and DCs (n = 3–4).
(H) Representative flow cytometric analysis of CD25 and CD44 expression of LSEC- or DC-primed CD8 T cells at 24 and 72 h after cross-priming.
(I) At 1 h after intravenous injection of ovalbumin (400 μg/mouse) or PBS (without OVA), murine livers and spleens were removed; LSECs and splenic DCs were isolated and co-cultured with naive OT-1 CD8 T cells for 24 h. Flow cytometry analysis of 2-NBDG uptake in CD8 T cells (n = 4).
(J) Number of LSEC-primed CD8 T cells at day 0, 1, and 3 after re-stimulation with CD3 alone or together with CD28 beads in the presence of IL-12 (n = 3). Data are representative of at least three separate experiments. ns, not significant; MFI, mean fluorescence intensity. Two-way ANOVA with Tukey's multiple comparison test (C, F, G, and I) and unpaired two-tailed t test (J). In (C, F, G, I, and J), data are mean ± SEM; errors are shown as SD.

use gene set enrichment analysis (GSEA) in a genome-wide transcriptome profile of LSEC-primed CD8 T cells (Böttcher et al., 2013) to look for the existence of T_{rm}-specific traits (Zhao et al., 2020). However, T_{rm}-specific genes were negatively enriched in LSEC-primed CD8 T cells that also lacked gene expression of CXCR6 (Figures S3J and S3K), a chemokine receptor pre-

dominantly expressed on hepatic T_{rm} (Fernandez-Ruiz et al., 2016). Expanding the analysis to other chemokine receptors like CXCR3, CX₃CR1, and CCR7 and to the lymph node homing marker CD62L showed that only the latter was highly upregulated in LSEC-primed CD8 T cells after 72 h of activation (Figure S3L). This indicated that LSEC-primed T cells constituted a

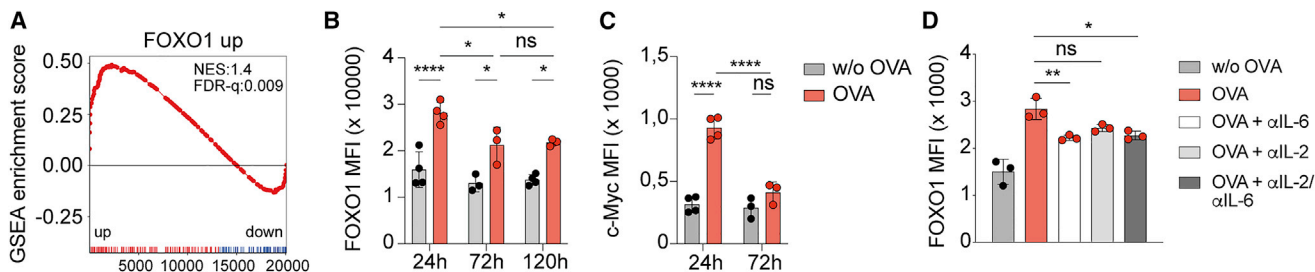


Figure 4. IL-6 mediates high FOXO1 expression in LSEC-primed CD8 T cells

(A) GSEA of DEGs of liver-primed CD8 T cells (Böttcher et al., 2013) using a gene set for upregulated genes in CD8 T cells from WT mice compared with FOXO1 KO mice³¹.

(B and C) FOXO1 and c-Myc expression levels in OT1 CD8 T cells at 24, 72 and 120 h after priming by LSECs (n = 3–4).

(D) FOXO1 expression levels in LSEC-primed CD8 T cells after incubation with blocking antibodies against IL-6 (10 μ g/mL) and IL-2 (10 μ g/mL) at 24 h after cross-priming (n = 3).

Data are representative of at least three separate experiments. ns, not significant; MFI, mean fluorescence intensity; NES, normalized enrichment score; FDR, false discovery rate. Two-way ANOVA with Tukey's multiple comparison test (B and C) and one-way ANOVA Tukey's multiple comparison test (D). In (B–D), data are mean \pm SEM; errors are shown as SD.

T cell population with memory-like function and unique metabolic properties that is distinct from T_{rm} . To verify whether these remarkable metabolic properties in LSEC-primed CD8 T cells allowed for functional responsiveness during antigen re-encounter, we stimulated these cells with anti-CD3/CD28-coated beads in the presence of IL-12. Clearly, LSEC-primed CD8 T cells rapidly secreted cytokines and robustly proliferated after stimulation (Figures 3I and S3M), consistent with a memory function. Together, these results indicate that LSEC-cross-primed CD8 T cells showed a unique metabolic profile characterized by an initial transient oxidative and glycolytic burst, which was followed by a functional memory-like state where cells responded to antigen re-encounter under inflammatory conditions.

Continuous FOXO1 expression in LSEC-primed CD8 T cells is dependent on IL-6 trans-signaling

The unique dynamic metabolic profile identified in LSEC-primed CD8 T cells is not compatible with current classifications of metabolic features characteristic for memory T cells or effector T cells (Buck et al., 2017) and led us to investigate molecular determinants of this differentiation. A prominent pathway that curbs T cell metabolism and plays an important role in control of immunity is programmed cell death protein 1 (PD-1)/programmed death-ligand 1 (PD-L1) signaling (Patsoukis et al., 2015). However, we did not find increased metabolic activity and a boosted phenotype in LSEC-primed CD8 T cells after 72 h in the presence of anti-PD-L1 blocking antibodies (Figures S4A and S4B), which excluded PD-1/PD-L1 signaling as major driver for the unique metabolic profile of LSEC-primed CD8 T cells. Another possibility of metabolic re-programming in T cells is through transcriptional regulation (Wang et al., 2011). One key transcription factor that determines the differentiation of T cells is FOXO1, and continuous FOXO1 expression supports memory T cell differentiation (Tejera et al., 2013). We therefore performed GSEA to evaluate enrichment of FOXO1-dependent genes (Hess Michelini et al., 2013) in LSEC-primed CD8 T cells compared with DC-primed CD8 T cells. Indeed, LSEC-primed CD8 T cells showed enrichment for FOXO1-dependent upregulated genes (Fig-

ure 4A), pointing toward regulation of T cell differentiation by FOXO1. Of note, CD62L, a known FOXO1 target gene, was among the genes found to be upregulated in LSEC-primed CD8 T cells. Elevated protein expression levels of FOXO1 found in LSEC-primed CD8 T cells at 24, 72, and 120 h after cross-priming by LSECs *in vitro* corroborated the results from GSEA (Figure 4B). However, increased FOXO1 expression in CD8 T cells during the initial phase of cross-priming (Figures S4D and S4E) was surprising, because FOXO1 phosphorylation through AKT in response to TCR signaling is considered to lead to nuclear export into the cytosol and proteasomal degradation of FOXO1 (Hedrick et al., 2012). We continued to investigate which transcription factor might have caused augmented metabolism shortly after cross-priming and checked for expression of c-Myc, a key transcription factor relevant for glycolysis in T cells (Wang et al., 2011). Indeed, we detected increased c-Myc levels at 24 h after T cell cross-priming and downregulation of c-Myc thereafter (Figure 4C), suggesting a transient role in controlling gene expression of key enzymes in the glycolytic pathway of LSEC-primed CD8 T cells.

Because IL-6 trans-signaling, a process where IL-6 bound to IL-6 receptors initiates signaling *in trans* (Fischer et al., 1997), operates in LSEC cross-priming of CD8 T cells (Böttcher et al., 2014) and IL-6-dependent Stat3 signaling prevents nuclear FOXO1 translocation into the cytosol for proteasomal degradation and thereby matures memory T cells (Oh et al., 2012), we reasoned that IL-6 may be important for FOXO1 expression in LSEC-primed CD8 T cells. Consequently, FOXO1 expression was significantly lower in the presence of anti-IL-6 blocking antibodies whereas c-Myc expression and phosphorylation levels of FOXO1 and Akt were unchanged (Figures 4D and S4F–4H), consistent with reduced FOXO1 degradation in LSEC-primed CD8 T cells. Gain-of-function experiments using hyper-IL-6, a cytokine complex consisting of IL-6 and IL-6-receptor-mediating IL-6 trans-signaling (Fischer et al., 1997), demonstrated increased FOXO1 expression in CD3-stimulated splenic CD8 T cells, and loss-of-function experiments using a pharmacological Stat3 inhibitor showed lower FOXO1 levels in LSEC-primed CD8 T cells (Figures S4I and S4J). Expression of the FOXO1

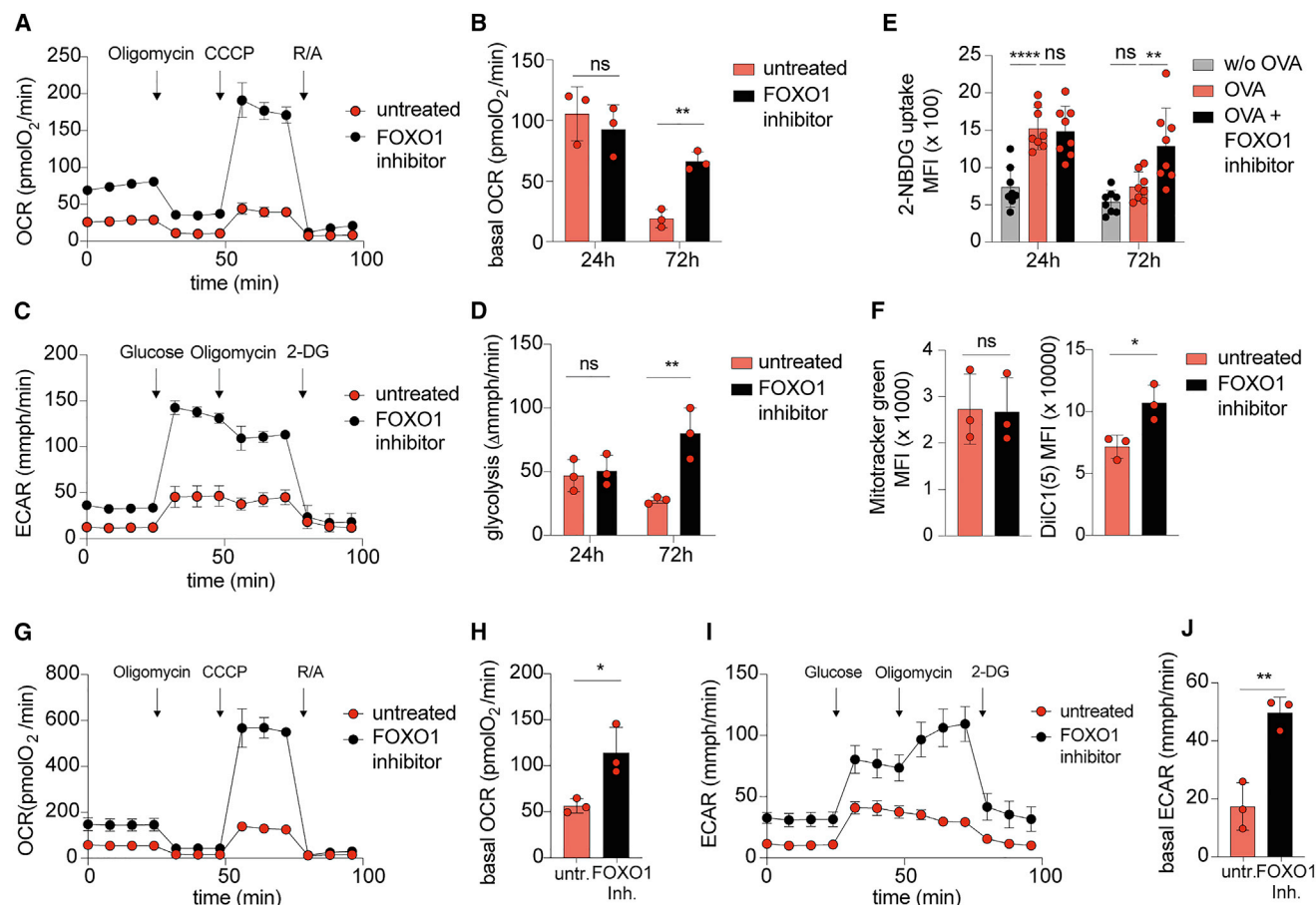


Figure 5. High FOXO1 activity dampens metabolic activity in LSEC-primed CD8 T cells after initial metabolic burst

(A–D) Representative profiles of OCR during mitochondrial stress test and ECAR during glucose stress test measured by extracellular flux analysis in OT1 CD8 T cells at 72 h after cross-priming by LSECs and treatment with FOXO1 inhibitor AS1842856 (100 nM) ($n = 3$).

(E) Analysis of glucose uptake with 2-NBDG in OT1 CD8 T cells at 24 and 72 h after priming by LSECs and treatment with AS1842856 ($n = 8$).

(F) Fluorescence intensity of MitoTracker Green and DilC1(5) in OT1 CD8 T cells at 72 h after cross-priming by LSECs treated with AS1842856 ($n = 3$).

(G–J) Representative profiles of OCR during mitochondrial stress test (G) and ECAR during glucose stress test (I) measured by extracellular flux analysis of in-vitro-differentiated memory CD8 T cells at day 6 treated with FOXO1 inhibitor AS1842856 (100 nM) for the last two days. Basal OCR (H) and basal ECAR (J) were quantified after consecutive injections of several compounds ($n = 3$).

Data are representative of at least three separate experiments. ns, not significant; MFI, mean fluorescence intensity; OCR, oxygen consumption rate; ECAR, extracellular acidification rate. Two-way ANOVA with Tukey's (B and D) and Dunnett's (E) multiple comparison test and unpaired two-tailed t test (F, H, and J). In (B, D, E, F, H, and J), data are mean \pm SEM; errors are shown as SD.

target gene CD62L was also reduced in IL-6-inhibited LSEC-primed CD8 T cells after 72 h, confirming reduced FOXO1 activity (Figure S4K). Interestingly, regulation of FOXO1 expression in LSEC-primed CD8 T cells was independent from IL-2 (Figure 4D), a key cytokine in hepatic T cell immunity (Benechet et al., 2019); rather, IL-2 promoted c-Myc expression in LSEC-primed CD8 T cells (Figure S4F). These results supported a role for IL-6 and Stat3 signaling in maintaining high FOXO1 expression in LSEC-primed CD8 T cells.

Transcriptional activity of FOXO1 controls metabolism in LSEC-primed CD8 T cells

Continuous activity of FOXO1 supports memory T cell formation and metabolic fitness of CD4 T cells (Newton et al., 2018), which led us to test whether FOXO1 activity shaped differentiation and

metabolism of LSEC-primed CD8 T cells. We applied an inhibitor of the transcriptional activity of FOXO1 (Nagashima et al., 2010) to co-cultures of cross-presenting LSECs and CD8 T cells and measured OXPHOS and glycolysis. Both metabolic pathways were unchanged after 24 h, but after 72 h of FOXO1 inhibition, OXPHOS and glycolysis dramatically increased in LSEC-primed CD8 T cells (Figures 5A–5E and S5A–S5E). In line, expression of genes coding for glycolytic enzymes, cellular glucose uptake, and mitochondrial membrane potential was increased after 72 h of FOXO1 inhibition in LSEC-primed CD8 T cells (Figures 5F and S5F). Importantly, FOXO1 inhibition in IL-15-treated splenic CD8 T cells, a well-established *in vitro* system studying metabolic parameters of memory T cells (Klein Geltink et al., 2017), caused similar metabolic enhancement as in LSEC-primed CD8 T cells, pointing toward a universal function of

FOXO1 in memory CD8 T cells to dampen metabolism (Figures 5G–5J, S5G, and S5H). Consequently, FOXO1-inhibited LSEC-primed CD8 T cells were unable to utilize exogenous FAs to generate ATP (Figure S5I), demonstrating defects in FAO that could curtail the longevity of memory T cells (Pan et al., 2017). Because FOXO1 activity in LSEC-primed CD8 T cells depended on IL-6 trans-signaling, we tested whether glycolytic activity in these cells was increased after 72 h of IL-6 inhibition. Similar to pharmacological inhibition of FOXO1 activity, IL-6 inhibition enhanced glycolysis (Figure S5J), suggesting that IL-6-induced FOXO1 activity was involved in downregulation of the metabolic activity in LSEC-primed CD8 T cells at late time points.

Enhanced glycolysis in LSEC-primed CD8 T cells with reduced FOXO1 activity is not coupled to effector T cell differentiation

Reducing FOXO1 activity in LSEC-primed CD8 T cells shifted cellular metabolism toward glycolysis, characteristic for an effector CD8 T cell metabolic profile, and led us to investigate whether increased glycolysis in FOXO1-inhibited LSEC-primed CD8 T cells was associated with effector T cell phenotype and function. Indeed, we found higher Ki67 and CD25 expression accompanied by increased release of IL-2 (Figures 6A–6C), suggesting higher proliferative capacity and activation status, both features of effector CD8 T cells. Increased metabolic activity was independent of IL-2 (Figure S6A), although IL-2 enhances glycolysis through increased expression of c-Myc (Preston et al., 2015). Increased glutamine metabolism, which promotes mTOR-dependent enforcement of glycolysis (Nakaya et al., 2014), may be involved in increased glycolysis, but we found only a slightly elevated gene expression of a glutamine transporter in LSEC-primed CD8 T cells after FOXO1 inhibition (Figure S6B). However, culturing FOXO1-inhibited LSEC-primed CD8 T cells in glutamine-free medium completely prevented the elevated glucose uptake, maximal mitochondrial respiration, and IL-2 release (Figures S6C–S6E), suggesting that glutamine was indispensable for metabolism in FOXO1-inhibited LSEC-primed CD8 T cells. Notwithstanding their dynamically regulated increased metabolic functions, LSEC-primed FOXO1-inhibited CD8 T cells failed to upregulate the transcription factor T-bet and did not kill target cells (Figures 6D, 6E, S6F, and 6G), demonstrating that transient high glycolytic activity was not directly linked to sustained T cell effector function. Furthermore, FOXO1-inhibited LSEC-primed T cells lost their capacity to secrete cytokines and to robustly proliferate and rapidly died after re-stimulation (Figures 6F and 6G, S6H–S6J). Similar effects were observed after neutralizing IL-6 in co-cultures of cross-priming LSECs and CD8 T cells (Figures S6K and S6L), suggesting defective memory T cell differentiation in the absence of IL-6-induced FOXO1 expression. Taken together, these results demonstrated an indispensable role of FOXO1 for control of metabolic features and induction of memory functions in LSEC-primed CD8 T cells.

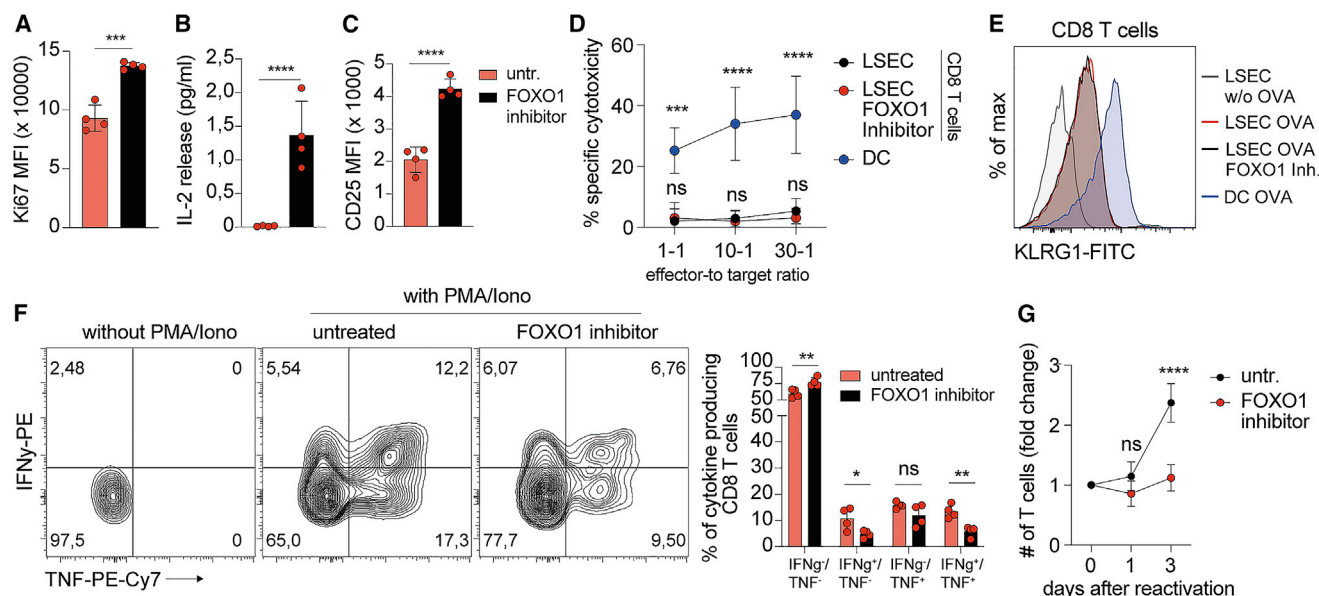
DISCUSSION

In this study we identified metabolic characteristics of antigen-presenting LSECs defined by high mitochondrial respiration in

combination with low glycolytic activity and revealed unique dynamics of cell metabolism in LSEC-primed CD8 T cells characterized by transient increase in glycolysis that was curtailed by IL-6-induced sustained FOXO1 transcription factor expression and required for memory cell features.

The liver provides a cornucopia of nutrients, including glucose (Rui, 2014), because of the metabolic activity of hepatocytes that assures stable local and systemic glucose levels during feeding and fasting conditions. Maintaining immune tolerance in this environment requires strict cell-intrinsic control of metabolism in immune cells, in contrast to environments with low glucose content, such as cancer tissue, where immune tolerance is enforced by nutrient deprivation (Chang et al., 2015). We found that LSECs, like most abundant liver-resident antigen-presenting cell populations, utilized various energy sources to support high-level mitochondrial OXPHOS, such as amino acids involving glutaminolysis, FAs involving β -oxidation, and glucose in the tricarboxylic acid (TCA) cycle. This illustrated a flexibility in substrate use of LSECs to fuel mitochondrial energy production. Metabolism in LSECs was linked to their function as liver-resident antigen-presenting cells, because inhibition of mitochondrial respiration led to a reduction of the scavenger function, which is critical for antigen cross-presentation (Schurich et al., 2009) and consequently reduced cross-presentation of endocytosed soluble antigens on MHC class I molecules to CD8 T cells. This demonstrated the catabolic demands of LSECs for high-level mitochondrial respiration to maintain their prominent immune features like antigen scavenging and cross-presentation to CD8 T cells (Limmer et al., 2000; Sorensen et al., 2012). However, there was also an anabolic demand for cross-presentation, for which LSECs required constitutive low-level glycolysis. Blocking glycolysis led to downregulation of both steady-state and LPS-induced MHC class I molecule expression in LSECs. The most likely explanation for this observation is that deoxyglucose inhibited utilization of glucose in the pentose phosphate pathway, which generates ribose-5-phosphates required for nucleotide synthesis and *de novo* expression of macromolecules (Stincone et al., 2015). These results suggest that MHC class I molecules in LSECs had a high turnover, which could explain that their steady-state, as well as *de novo*, expression after LPS stimulation was sensitive to deoxyglucose. After LPS stimulation, *de novo* cytokine production, such as IL-6, also depended on low-level glycolysis. LSEC-released IL-6 helps to mount innate immunity against hepatotropic infections and serves as a co-stimulatory signal for T cells in the absence of expression of canonical co-stimulatory molecules (Böttcher et al., 2014). Importantly, IL-6 and Stat3 signaling support the longevity of memory CD8 T cells (Cui et al., 2011), which may explain the capacity of IL-6 trans-signaling by cross-priming LSECs to program naive CD8 T cells into memory CD8 T cells, despite absence of canonical co-stimulation.

Beyond the contribution of metabolism to cross-presentation for CD8 T cells, we found that LSECs did not increase their glycolytic activity after LPS stimulation, which is different from the immunogenic response of DCs to LPS challenge (Everts et al., 2014). A possible explanation for this lack of functional maturation after LPS stimulation may be the ultrastructure of mitochondria in LSECs, which show highly condensed mitochondrial



cristae. This may result from reduced mitochondrial fission that is known to increase efficiency of mitochondrial respiration but curtail glycolytic activity in immune cells (Buck et al., 2016). Along this line, pharmacological inhibition of mitochondrial fission in DCs prevents LPS-induced increase of glycolysis and maturation (Everts et al., 2014). Moreover, direct activation of mTOR signaling, which increases glycolysis in monocytes/macrophages (Cheng et al., 2014), failed to increase glycolytic activity in LSECs. This indicates a cell-intrinsic block to increase glycolytic activity even in the presence of high glucose levels and gut-derived LPSs in portal venous blood and to preserve non-immunogenic function of LSECs in the liver microenvironment.

In contrast to antigen-presenting LSECs, LPS-matured glycolytic DCs cross-prime CD8 T cells to become effector CD8 T cells, which is associated with re-programming of T cell metabolism toward glycolysis (Everts et al., 2014). Whereas immature DCs with low glycolytic activity direct naive CD8 T cells to become anergic or die, low-glycolytic LSECs cause differentiation of CD8 T cells into memory T cells via IL-6 trans-signaling (Böttcher et al., 2014). We found the signaling pathways instructing LSEC-primed CD8 T cells to develop into memory T cells to involve a unique dynamic of transient high mitochondrial respiration and glycolysis followed by rapid downregulation of both metabolic pathways. These dynamics of metabolism in LSEC-primed CD8 T cells are unique and not compatible with our current understanding of

metabolism in effector and memory CD8 T cells. Mitochondrial ATP is necessary for robust T cell activation (Chang et al., 2013), indicating that high initial mitochondrial respiration in LSEC-primed CD8 T cells coincided with TCR signaling from efficient antigen presentation. The rapid yet transient increase in metabolic activity supported by initial high c-Myc expression may provide the necessary bioenergetic building blocks and energy to facilitate execution of transient effector functions in LSEC-primed CD8 T cells.

Beyond these unique dynamics of metabolism, LSEC-primed CD8 T cells were distinct from canonical central-memory T cells, which employ FAO to fuel functions and achieve cell longevity (Pearce et al., 2009). We found that LSEC-primed CD8 T cells lacked spare respiratory capacity (SRC), which is considered to be required for memory T cells to mount a rapid response during antigen re-encounter (van der Windt et al., 2012). Along this line, re-activation of LSEC-primed CD8 T cells for induction of effector function was slower and required combinatorial stimulation through TCR, CD28, and IL-12, which may relate to this difference of SRC in LSEC-primed CD8 T cells compared with conventional memory cells. Importantly, LSEC-primed CD8 T cells utilized exogenous FAs instead of endogenous FAs to fuel FAO, which resembles a metabolic feature of T_{rm} (Pan et al., 2017). However, the lack of rapid cytotoxic function after antigen encounter, absence of the tissue-resident marker CXCR6, and a missing T_{rm} gene signature all suggested that LSEC-primed CD8 T cells constituted a separate population of memory T cells that

remains non-responsive during steady state and supports induction of immunity during inflammation.

The molecular mechanisms mediating induction of these unique memory CD8 T cells through cross-priming LSECs were also distinct from induction of canonical memory CD8 T cells. Pharmacological inhibition of mTOR enhances memory cell formation and inhibition of nuclear localization of FOXO1, which promotes induction of memory rather than effector CD8 T cells (Araki et al., 2009; Hedrick et al., 2012). However, the metabolic impact of FOXO1 during T cell differentiation had not been investigated. Here, we demonstrate that FOXO1 constrained metabolism in LSEC-primed memory CD8 T cells and determined survival, proliferation, and cytokine release after re-activation. This suggested that FOXO1 regulated metabolic fitness not only in conventional and regulatory CD4 T cells (Newton et al., 2018) but also in LSEC-primed memory CD8 T cells. However, because LSECs constitutively expressed FOXO1, we cannot formally exclude a role of LSEC-expressed FOXO1 for phenotype and function of LSEC-primed T cells. In contrast to the current understanding of T cell effector function, high metabolic activity in LSEC-primed CD8 T cells after down-regulation of FOXO1 was not associated with induction of effector function, which may be related to absence of transcription factors like T-bet that determine expression of effector molecules (Intlekofer et al., 2005) or subcritical intracellular levels of metabolites, such as acetyl-coenzyme A (CoA), that regulate gene transcription at the epigenetic level (Peng et al., 2016). Our results demonstrated that IL-6 trans-signaling and Stat3 signaling induced high FOXO1 expression in LSEC-primed CD8 T cells and thereby contributed to memory cell formation. It is likely that the IL-6-induced high FOXO1 activity determined longevity of LSEC-primed CD8 T cells, whereas signaling through co-stimulatory molecules like CD28 and IL-12 triggered further differentiation of LSEC-primed memory CD8 T cells into effector cells. Besides promoting cell longevity, IL-6-enforced FOXO1 expression in LSEC-primed CD8 T cells might be important for preventing the generation of auto-aggressive CD8 T cells, which arise when low transcriptional activity of FOXO1 is present in CD8 T cells and cause severe liver damage (Dudek et al., 2021). The unique dynamics of metabolism in LSEC-primed CD8 T cells mediated by IL-6-induced high FOXO1 activity may therefore maintain immune tolerance during steady-state situations in the liver while still allowing T cell immunity to be generated upon induction of inflammation.

Limitations of the study

Concerning potential limitations of this study, like most investigations on immunological functions of liver-resident cell populations, our results are limited to preclinical models that allow for isolation of the liver cell populations and their phenotypic and functional characterization. However, previous studies have demonstrated that mechanistic principles of immune regulation through liver-resident cell populations are often similar between preclinical models and humans (Dudek et al., 2021; Pfister et al., 2021). For a formal proof that human LSECs share similar metabolic and immune-functional properties with murine LSECs, experiments with primary LSECs from human liver material need to be performed.

STAR★METHODS

Detailed methods are provided in the online version of this paper and include the following:

- **KEY RESOURCE TABLE**
- **RESOURCE AVAILABILITY**
 - Lead contact
 - Materials availability
 - Data and code availability
- **EXPERIMENTAL MODEL AND SUBJECT DETAILS**
- **METHOD DETAILS**
 - Isolation and culture of primary cell populations from liver and spleen
 - Stimulation of CD8 T cells *in vitro*
 - Flow cytometry
 - Analysis of T cell effector functions
 - Determination of cellular bioenergetics
 - Transmission electron microscopy
 - Quantitative real-time PCR
 - Geneset enrichment analysis (GSEA)
- **QUANTIFICATION AND STATISTICAL ANALYSIS**

SUPPLEMENTAL INFORMATION

Supplemental information can be found online at <https://doi.org/10.1016/j.celrep.2022.110389>.

ACKNOWLEDGMENTS

This work was supported by a grant from the DFG (SFB-TRR-179) and the German Center for Infection Research, Munich branch.

AUTHOR CONTRIBUTIONS

M.D. and K.L. contributed equally to this work; M.D., K.L., T.B., M.L., S.H., S.M., A.Y., L.D., C.E., B.P., M.P., and S.M. performed experiments and analyzed the data; S.R.-J. provided essential reagents; S.D. performed bioinformatic analysis; and H.Z., M.D., K.L., and P.A.K. wrote the manuscript.

DECLARATION OF INTERESTS

The authors declare no competing interests.

Received: May 3, 2021

Revised: November 16, 2021

Accepted: January 25, 2022

Published: February 15, 2022

REFERENCES

- Andrade, J., Shi, C., Costa, A.S.H., Choi, J., Kim, J., Doddaballapur, A., Sugin, T., Ong, Y.T., Castro, M., Zimmermann, B., et al. (2021). Control of endothelial quiescence by FOXO-regulated metabolites. *Nat. Cell Biol.* 23, 413–423. <https://doi.org/10.1038/s41556-021-00637-6>.
- Araki, K., Turner, A.P., Shaffer, V.O., Gangappa, S., Keller, S.A., Bachmann, M.F., Larsen, C.P., and Ahmed, R. (2009). mTOR regulates memory CD8 T-cell differentiation. *Nature* 460, 108–112.
- Balmer, M.L., Slack, E., de Gottardi, A., Lawson, M.A., Hapfelmeier, S., Miele, L., Grieco, A., Van Vlierberghe, H., Fahrner, R., Patuto, N., et al. (2014). The liver may act as a firewall mediating mutualism between the host and its gut commensal microbiota. *Sci. Transl. Med.* 6, 237ra266. <https://doi.org/10.1126/scitranslmed.3008618>.

- Benechet, A.P., De Simone, G., Di Lucia, P., Cilenti, F., Barbiera, G., Le Bert, N., Fumagalli, V., Lusito, E., Moalli, F., Bianchessi, V., et al. (2019). Dynamics and genomic landscape of CD8(+) T cells undergoing hepatic priming. *Nature* 574, 200–205. <https://doi.org/10.1038/s41586-019-1620-6>.
- Böttcher, J.P., Schanz, O., Garbers, C., Zaremba, A., Hegenbarth, S., Kurts, C., Beyer, M., Schultze, J.L., Kastenmüller, W., Rose-John, S., and Knolle, P.A. (2014). IL-6 trans-signaling-dependent rapid development of cytotoxic CD8(+) T cell function. *Cell Rep.* 8, 1318–1327. <https://doi.org/10.1016/j.celrep.2014.07.008>.
- Böttcher, J.P., Schanz, O., Wohleber, D., Abdullah, Z., Debey-Pascher, S., Staratschek-Jox, A., Höchst, B., Hegenbarth, S., Grell, J., Limmer, A., et al. (2013). Liver-primed memory T cells generated under noninflammatory conditions provide anti-infectious immunity. *Cell Rep.* 3, 779–795. <https://doi.org/10.1016/j.celrep.2013.02.008>.
- Buck, M.D., O'Sullivan, D., Klein Geltink, R.I., Curtis, J.D., Chang, C.H., Sanin, D.E., Qiu, J., Kretz, O., Braas, D., van der Windt, G.J., et al. (2016). Mitochondrial dynamics controls T cell fate through metabolic programming. *Cell* 166, 63–76. <https://doi.org/10.1016/j.cell.2016.05.035>.
- Buck, M.D., Sowell, R.T., Kaech, S.M., and Pearce, E.L. (2017). Metabolic instruction of immunity. *Cell* 169, 570–586. <https://doi.org/10.1016/j.cell.2017.04.004>.
- Carambia, A., Freund, B., Schwinge, D., Bruns, O.T., Salmen, S.C., Ittrich, H., Reimer, R., Heine, M., Huber, S., Waurisch, C., et al. (2015). Nanoparticle-based autoantigen delivery to Treg-inducing liver sinusoidal endothelial cells enables control of autoimmunity in mice. *J. Hepatol.* 62, 1349–1356. <https://doi.org/10.1016/j.jhep.2015.01.006>.
- Chang, C.H., Curtis, J.D., Maggi, L.B., Jr., Faubert, B., Villarino, A.V., O'Sullivan, D., Huang, S.C., van der Windt, G.J., Blagih, J., Qiu, J., et al. (2013). Post-transcriptional control of T cell effector function by aerobic glycolysis. *Cell* 153, 1239–1251. <https://doi.org/10.1016/j.cell.2013.05.016>.
- Chang, C.H., Qiu, J., O'Sullivan, D., Buck, M.D., Noguchi, T., Curtis, J.D., Chen, Q., Gindin, M., Gubin, M.M., van der Windt, G.J., et al. (2015). Metabolic competition in the tumor microenvironment is a driver of cancer progression. *Cell* 162, 1229–1241. <https://doi.org/10.1016/j.cell.2015.08.016>.
- Cheng, S.C., Quintin, J., Cramer, R.A., Shephardson, K.M., Saeed, S., Kumar, V., Giamarellos-Bourboulis, E.J., Martens, J.H., Rao, N.A., Aghajani-efah, A., et al. (2014). mTOR- and HIF-1 α -mediated aerobic glycolysis as metabolic basis for trained immunity. *Science* 345, 1250684. <https://doi.org/10.1126/science.1250684>.
- Crispe, I.N. (2014). Immune tolerance in liver disease. *Hepatology* 60, 2109–2117. <https://doi.org/10.1002/hep.27254>.
- Cui, W., Liu, Y., Weinstein, J.S., Craft, J., and Kaech, S.M. (2011). An interleukin-21-interleukin-10-STAT3 pathway is critical for functional maturation of memory CD8+ T cells. *Immunity* 35, 792–805. <https://doi.org/10.1016/j.immuni.2011.09.017>.
- Diehl, L., Schurich, A., Grochtmann, R., Hegenbarth, S., Chen, L., and Knolle, P.A. (2008). Tolerogenic maturation of liver sinusoidal endothelial cells promotes B7-homolog 1-dependent CD8+ T cell tolerance. *Hepatology* 47, 296–305. <https://doi.org/10.1002/hep.21965>.
- Dudek, M., Pfister, D., Donakonda, S., Filpe, P., Schneider, A., Laschinger, M., Hartmann, D., Huser, N., Meiser, P., Bayerl, F., et al. (2021). Auto-aggressive CXCR6(+) CD8 T cells cause liver immune pathology in NASH. *Nature* 592, 444–449. <https://doi.org/10.1038/s41586-021-03233-8>.
- Everts, B., Amiel, E., Huang, S.C., Smith, A.M., Chang, C.H., Lam, W.Y., Redmann, V., Freitas, T.C., Blagih, J., van der Windt, G.J., et al. (2014). TLR-driven early glycolytic reprogramming via the kinases TBK1-IKK ϵ supports the anabolic demands of dendritic cell activation. *Nat. Immunol.* 15, 323–332. <https://doi.org/10.1038/ni.2833>.
- Fernandez-Ruiz, D., Ng, W.Y., Holz, L.E., Ma, J.Z., Zaid, A., Wong, Y.C., Lau, L.S., Mollard, V., Cozijnsen, A., Collins, N., et al. (2016). Liver-resident memory CD8+ T cells form a front-line defense against malaria liver-stage infection. *Immunity* 45, 889–902. <https://doi.org/10.1016/j.immuni.2016.08.011>.
- Fischer, M., Goldschmitt, J., Peschel, C., Brakenhoff, J.P., Kallen, K.J., Wollmer, A., Grotzinger, J., and Rose-John, S. (1997). I. A bioactive designer cytokine for human hematopoietic progenitor cell expansion. *Nat. Biotechnol.* 15, 142–145. <https://doi.org/10.1038/nbt0297-142>.
- Fox, C.J., Hammerman, P.S., and Thompson, C.B. (2005). Fuel feeds function: energy metabolism and the T-cell response. *Nat. Rev. Immunol.* 5, 844–852. <https://doi.org/10.1038/nri1710>.
- Frauwirth, K.A., Riley, J.L., Harris, M.H., Parry, R.V., Rathmell, J.C., Plas, D.R., Elstrom, R.L., June, C.H., and Thompson, C.B. (2002). The CD28 signaling pathway regulates glucose metabolism. *Immunity* 16, 769–777.
- Ganeshan, K., and Chawla, A. (2014). Metabolic regulation of immune responses. *Annu. Rev. Immunol.* 32, 609–634. <https://doi.org/10.1146/annurev-immunol-032713-120236>.
- Hedrick, S.M., Hess Michelini, R., Doedens, A.L., Goldrath, A.W., and Stone, E.L. (2012). FOXO transcription factors throughout T cell biology. *Nat. Rev. Immunol.* 12, 649–661. <https://doi.org/10.1038/nri3278>.
- Hess Michelini, R., Doedens, A.L., Goldrath, A.W., and Hedrick, S.M. (2013). Differentiation of CD8 memory T cells depends on Foxo1. *J. Exp. Med.* 210, 1189–1200. <https://doi.org/10.1084/jem.20130392>.
- Horton, C., Shanmugarajah, K., and Fairchild, P.J. (2017). Harnessing the properties of dendritic cells in the pursuit of immunological tolerance. *Biomed. J.* 40, 80–93. <https://doi.org/10.1016/j.bj.2017.01.002>.
- Intlekofer, A.M., Takemoto, N., Wherry, E.J., Longworth, S.A., Northrup, J.T., Palanivel, V.R., Mullen, A.C., Gasink, C.R., Kaech, S.M., Miller, J.D., et al. (2005). Effector and memory CD8+ T cell fate coupled by T-bet and eomesodermin. *Nat. Immunol.* 6, 1236–1244. <https://doi.org/10.1038/ni1268>.
- Khan, O., Giles, J.R., McDonald, S., Manne, S., Ngiew, S.F., Patel, K.P., Werner, M.T., Huang, A.C., Alexander, K.A., Wu, J.E., et al. (2019). TOX transcriptionally and epigenetically programs CD8(+) T cell exhaustion. *Nature* 571, 211–218. <https://doi.org/10.1038/s41586-019-1325-x>.
- Klein Geltink, R.I., O'Sullivan, D., Corrado, M., Bremser, A., Buck, M.D., Buescher, J.M., Firat, E., Zhu, X., Niedermann, G., Caputa, G., et al. (2017). Mitochondrial priming by CD28. *Cell* 171, 385–397 e311. <https://doi.org/10.1016/j.cell.2017.08.018>.
- Liberman, E.A., Topaly, V.P., Tsofin, L.M., Jasaitis, A.A., and Skulachev, V.P. (1969). Mechanism of coupling of oxidative phosphorylation and the membrane potential of mitochondria. *Nature* 222, 1076–1078.
- Limmer, A., Ohl, J., Kurts, C., Ljunggren, H.G., Reiss, Y., Groettrup, M., Momberg, F., Arnold, B., and Knolle, P.A. (2000). Efficient presentation of exogenous antigen by liver endothelial cells to CD8+ T cells results in antigen-specific T-cell tolerance. *Nat. Med.* 6, 1348–1354.
- Nagashima, T., Shigematsu, N., Maruki, R., Urano, Y., Tanaka, H., Shimaya, A., Shimokawa, T., and Shibasaki, M. (2010). Discovery of novel forkhead box O1 inhibitors for treating type 2 diabetes: improvement of fasting glycemia in diabetic db/db mice. *Mol. Pharmacol.* 78, 961–970. <https://doi.org/10.1124/mol.110.065714>.
- Nakaya, M., Xiao, Y., Zhou, X., Chang, J.H., Chang, M., Cheng, X., Blonska, M., Lin, X., and Sun, S.C. (2014). Inflammatory T cell responses rely on amino acid transporter ASCT2 facilitation of glutamine uptake and mTORC1 kinase activation. *Immunity* 40, 692–705. <https://doi.org/10.1016/j.immuni.2014.04.007>.
- Newton, R.H., Shrestha, S., Sullivan, J.M., Yates, K.B., Compeer, E.B., Ron-Harel, N., Blazar, B.R., Bensinger, S.J., Haining, W.N., Dustin, M.L., et al. (2018). Maintenance of CD4 T cell fitness through regulation of Foxo1. *Nat. Immunol.* 19, 838–848. <https://doi.org/10.1038/s41590-018-0157-4>.
- O'Neill, L.A., and Hardie, D.G. (2013). Metabolism of inflammation limited by AMPK and pseudo-starvation. *Nature* 493, 346–355. <https://doi.org/10.1038/nature11862>.
- O'Neill, L.A., and Pearce, E.J. (2016). Immunometabolism governs dendritic cell and macrophage function. *J. Exp. Med.* 213, 15–23. <https://doi.org/10.1084/jem.20151570>.
- Oh, H.M., Yu, C.R., Dambaza, I., Marrero, B., and Egwuagu, C.E. (2012). STAT3 protein interacts with Class O Forkhead transcription factors in the

- p cytoplasm and regulates nuclear/cytoplasmic localization of FoxO1 and FoxO3a proteins in CD4(+) T cells.
- J. Biol. Chem.*
- 287, 30436–30443.
- <https://doi.org/10.1074/jbc.M112.359661>
- .
- Pallett, L.J., Gill, U.S., Quaglia, A., Sinclair, L.V., Jover-Cobos, M., Schurich, A., Singh, K.P., Thomas, N., Das, A., Chen, A., et al. (2015). Metabolic regulation of hepatitis B immunopathology by myeloid-derived suppressor cells. *Nat. Med.* 21, 591–600. <https://doi.org/10.1038/nm.3856>.
- Pan, Y., and Kupper, T.S. (2018). Metabolic reprogramming and longevity of tissue-resident memory T cells. *Front. Immunol.* 9, 1347. <https://doi.org/10.3389/fimmu.2018.01347>.
- Pan, Y., Tian, T., Park, C.O., Lofftus, S.Y., Mei, S., Liu, X., Luo, C., O'Malley, J.T., Gehad, A., Teague, J.E., et al. (2017). Survival of tissue-resident memory T cells requires exogenous lipid uptake and metabolism. *Nature* 543, 252–256. <https://doi.org/10.1038/nature21379>.
- Patsoukis, N., Bardhan, K., Chatterjee, P., Sari, D., Liu, B., Bell, L.N., Karoly, E.D., Freeman, G.J., Petkova, V., Seth, P., et al. (2015). PD-1 alters T-cell metabolic reprogramming by inhibiting glycolysis and promoting lipolysis and fatty acid oxidation. *Nat. Commun.* 6, 6692. <https://doi.org/10.1038/ncomms7692>.
- Pearce, E.L., Poffenberger, M.C., Chang, C.H., and Jones, R.G. (2013). Fueling immunity: insights into metabolism and lymphocyte function. *Science* 342, 1242454. <https://doi.org/10.1126/science.1242454>.
- Pearce, E.L., Walsh, M.C., Cejas, P.J., Harms, G.M., Shen, H., Wang, L.S., Jones, R.G., and Choi, Y. (2009). Enhancing CD8 T-cell memory by modulating fatty acid metabolism. *Nature* 460, 103–107. <https://doi.org/10.1038/nature08097>.
- Peng, M., Yin, N., Chhangawala, S., Xu, K., Leslie, C.S., and Li, M.O. (2016). Aerobic glycolysis promotes T helper 1 cell differentiation through an epigenetic mechanism. *Science* 354, 481–484. <https://doi.org/10.1126/science.aaf6284>.
- Pfister, D., Nunez, N.G., Pinyol, R., Govaere, O., Pinter, M., Szydlowska, M., Gupta, R., Qiu, M., Deczkowska, A., Weiner, A., et al. (2021). NASH limits anti-tumour surveillance in immunotherapy-treated HCC. *Nature* 592, 450–456. <https://doi.org/10.1038/s41586-021-03362-0>.
- Preston, G.C., Sinclair, L.V., Kaskar, A., Hukelmann, J.L., Navarro, M.N., Ferrero, I., MacDonald, H.R., Cowling, V.H., and Cantrell, D.A. (2015). Single cell tuning of Myc expression by antigen receptor signal strength and interleukin-2 in T lymphocytes. *EMBO J.* 34, 2008–2024. <https://doi.org/10.15252/embj.201490252>.
- Ritchie, M.E., Phipson, B., Wu, D., Hu, Y., Law, C.W., Shi, W., and Smyth, G.K. (2015). Limma powers differential expression analyses for RNA-sequencing and microarray studies. *Nucleic Acids Res.* 43, e47. <https://doi.org/10.1093/nar/gkv007>.
- Rui, L. (2014). Energy metabolism in the liver. *Compr. Physiol.* 4, 177–197. <https://doi.org/10.1002/cphy.c130024>.
- Schurich, A., Bottcher, J.P., Burgdorf, S., Penzler, P., Hegenbarth, S., Kern, M., Dolf, A., Endl, E., Schultze, J., Wiertz, E., et al. (2009). Distinct kinetics and dynamics of cross-presentation in liver sinusoidal endothelial cells compared to dendritic cells. *Hepatology* 50, 909–919. <https://doi.org/10.1002/hep.23075>.
- Schurich, A., Pallett, L.J., Lubowiecki, M., Singh, H.D., Gill, U.S., Kennedy, P.T., Nastouli, E., Tanwar, S., Rosenberg, W., and Maini, M.K. (2013). The third signal cytokine IL-12 rescues the anti-viral function of exhausted HBV-specific CD8 T cells. *PLoS Pathog.* 9, e1003208. <https://doi.org/10.1371/journal.ppat.1003208>.
- Sorensen, K.K., McCourt, P., Berg, T., Crossley, C., Le Couteur, D., Wake, K., and Smedsrod, B. (2012). The scavenger endothelial cell: a new player in homeostasis and immunity. *Am. J. Physiol. Regul. Integr. Comp. Physiol.* 303, R1217–R1230. <https://doi.org/10.1152/ajpregu.00686.2011>.
- Stincone, A., Prigione, A., Cramer, T., Wamelink, M.M., Campbell, K., Cheung, E., Olin-Sandoval, V., Gruning, N.M., Kruger, A., Tauqeer Alam, M., et al. (2015). The return of metabolism: biochemistry and physiology of the pentose phosphate pathway. *Biol. Rev. Camb. Phil. Soc.* 90, 927–963. <https://doi.org/10.1111/brv.12140>.
- Subramanian, A., Tamayo, P., Mootha, V.K., Mukherjee, S., Ebert, B.L., Gillette, M.A., Paulovich, A., Pomeroy, S.L., Golub, T.R., Lander, E.S., and Mesirov, J.P. (2005). Gene set enrichment analysis: a knowledge-based approach for interpreting genome-wide expression profiles. *Proc. Natl. Acad. Sci. U S A* 102, 15545–15550. <https://doi.org/10.1073/pnas.0506580102>.
- Tejera, M.M., Kim, E.H., Sullivan, J.A., Plisch, E.H., and Suresh, M. (2013). FoxO1 controls effector-to-memory transition and maintenance of functional CD8 T cell memory. *J. Immunol.* 191, 187–199. <https://doi.org/10.4049/jimmunol.1300331>.
- Thomson, A.W., and Knolle, P.A. (2010). Antigen-presenting cell function in the tolerogenic liver environment. *Nat. Rev. Immunol.* 10, 753–766. <https://doi.org/10.1038/nri2858>.
- van der Windt, G.J., Everts, B., Chang, C.H., Curtis, J.D., Freitas, T.C., Amiel, E., Pearce, E.J., and Pearce, E.L. (2012). Mitochondrial respiratory capacity is a critical regulator of CD8+ T cell memory development. *Immunity* 36, 68–78. <https://doi.org/10.1016/j.immuni.2011.12.007>.
- Wang, R., Dillon, C.P., Shi, L.Z., Milasta, S., Carter, R., Finkelstein, D., McCormick, L.L., Fitzgerald, P., Chi, H., Munger, J., and Green, D.R. (2011). The transcription factor Myc controls metabolic reprogramming upon T lymphocyte activation. *Immunity* 35, 871–882. <https://doi.org/10.1016/j.immuni.2011.09.021>.
- Wilhelm, K., Happel, K., Eelen, G., Schoors, S., Oellerich, M.F., Lim, R., Zimmermann, B., Aspalter, I.M., Franco, C.A., Boettger, T., et al. (2016). FOXO1 couples metabolic activity and growth state in the vascular endothelium. *Nature* 529, 216–220. <https://doi.org/10.1038/nature16498>.
- Zhao, J., Zhang, S., Liu, Y., He, X., Qu, M., Xu, G., Wang, H., Huang, M., Pan, J., Liu, Z., et al. (2020). Single-cell RNA sequencing reveals the heterogeneity of liver-resident immune cells in human. *Cell Discov.* 6, 22. <https://doi.org/10.1038/s41421-020-0157-z>.

STAR★METHODS

KEY RESOURCE TABLE

REAGENT or RESOURCE	SOURCE	IDENTIFIER
Antibodies		
Anti-mouse CD146 (clone ME-9F19)	Biologend	# 134706
Anti-mouse CD54 (clone 3E2)	BD Bioscience	# 553253
Anti-mouse CD106 (clone C1429)	Biologend	# 105722
Anti-mouse H2k ^b (clone Rea932)	Miltenyi Biotec	#130-115-490
Anti-mouse MHC II (M5/114.15.2)	Thermo Fisher	# 12-5321-82
Anti-mouse CD80 (clone 16-10A1)	Biologend	# 104734
Anti-mouse CD86 (clone GL1)	Biologend	# 105028
Anti-mouse CD40 (clone 3/23)	Biologend	# 124626
Anti-mouse OX40L (clone RM134L)	Biologend	# 108806
Anti-mouse CD8a (clone 53-6.7)	Biologend	# 100752
Anti-mouse CD25 (clone PC61.5)	Thermo Fisher	# 17-0251-82
Anti-mouse PD-1 (clone 29F.1A12)	Biologend	# 135218
Anti-mouse CD44 (clone IM7)	Biologend	# 103032
Anti-mouse CD62L (clone MEL-14)	Biologend	# 104424
Anti-mouse CD186 (clone SA051D1)	Biologend	# 151109
Anti-mouse CCR7 (clone 4B12)	Thermo Fisher	# 48-1971-82
Anti-mouse CX3CR1 (clone SA011F11)	Biologend	# 149016
Anti-mouse CXCR3 (clone CXCR3-173)	Biologend	# 126514
Anti-mouse KLRG1 (clone 2F1)	Biologend	# 138410
Anti-mouse FOXO1 (clone C29H4)	Cell Signaling	# 2880S
Anti-mouse IFN γ (clone XM61.2)	Thermo Fisher	# 48-7311-82
Anti-mouse pFOXO1 (clone Ser256)	Cell Signaling	# 9461S
Anti-mouse pAkt (clone SDRNR)	Thermo Fisher	# 17-9715-42
Anti-mouse c-Myc (clone D84C12)	Cell Signaling	# 5605S
Anti-mouse TNF (clone MP6-XT22)	Thermo Fisher	# 25-7321-82
Anti-human Granzyme B (cross-reactive with mouse, clone GRB04)	Thermo Fisher	# GRB04
Anti-mouse Bcl-2 (clone 100)	Biologend	# 658709
Anti-mouse EOMES (clone Dan11mag)	Thermo Fisher	# 12-4875-82
Anti-mouse T-bet (clone eBio4B10)	Thermo Fisher	# 25-5825-82
Anti-mouse Ki67 (clone 11F6)	Biologend	# 151210
Goat anti-Rabbit IgG (H+L) Cross-Adsorbed Secondary Antibody, Alexa Fluor 647	Thermo Fisher	# A-21244
Anti-rabbit IgG (H+L), F(ab') ₂ Fragment (Alexa Fluor® 488 Conjugate)	Cell Signaling	# 4412S
Anti-mouse IL-2 ELISA Kit	Thermo Fisher	# BMS601
Anti-mouse IL-6 ELISA Kit	Thermo Fisher	# BMS603-2
Chemicals, peptides, and recombinant proteins		
MitoTracker™ Green FM	Thermo Fisher	# M7514
MitoProbe™ DiIC ₁ (5) Assay Kit	Thermo Fisher	# M34151
Low Density Lipoprotein From Human Plasma, Acetylated, Alexa Fluor™ 488 Conjugate	Thermo Fisher	# L23380
Purified anti-mouse IL-6 Antibody	Biologend	# 504502

(Continued on next page)

Continued

REAGENT or RESOURCE	SOURCE	IDENTIFIER
IL-2 Monoclonal Antibody (S4B6), Functional Grade	Thermo Fisher	# 16-7020-85
CD274 (PD-L1, B7-H1), Monoclonal Antibody (MIH5)	Thermo Fisher	# 14-5982-82
FOXO1 inhibitor AS1842856	Merck	# 344355
UK5099	Sigma	# PZ0160
BPTES	Sigma	# SML0601
Etomoxir	Sigma	# 236020
Oligomycin	Merck	# 495455
2-Deoxy-D-glucose	Merck	# 25972
Rotenone	Sigma	# R8875
CCCP	Sigma	# 215911
Antimycin-A	Sigma	# A8674
Ovalbumin	Sigma	# A5503
Ovalbumin, Alexa Fluor™ 647 Conjugate	Thermo Fisher	# O34784
Mouse IL-15/IL-15R Complex Recombinant Protein	Thermo Fisher	# 14-8152-80
Recombinant Human TGF-β1 (cross-reactive with mouse)	Peprtech	# 100-21
Foxp3/Transcription Factor Staining Buffer Set	Thermo Fisher	# 00-5523-00
2-NBDG	Thermo Fisher	# N13195
MHY1485	Calbiochem	# 5005540001
DAPT	Tocris	# 2634
Seahorse XF RPMI medium	Agilent	# 103576-100
Seahorse XF base medium	Agilent	# 103335-100
CD146 (LSEC) MicroBeads, mouse	Miltenyi Biotec	# 130-092-007
CD11c MicroBeads UltraPure, mouse	Miltenyi Biotec	# 130-125-835
Naive CD8a ⁺ T Cell Isolation Kit, mouse	Miltenyi Biotec	# 130-096-543
CD8a (Ly-2) MicroBeads, mouse	Miltenyi Biotec	# 130-117-044
Dynabeads™ Mouse T-Activator CD3/CD28 for T-Cell Expansion and Activation	Thermo Fisher	# 11452D
Recombinant Murine IL-12 p70	Peprtech	# 210-12
OVA 257-264	InvivoGen	# vac-sin
Purified anti-mouse CD3ε Antibody	Biolegend	# 100302

Critical commercial assays

XF Long Chain Fatty Acid Oxidation Stress Test Kit	Agilent	# 103672-100
--	---------	--------------

Experimental models: Organisms/strains

Mouse: male C57BL/6	Charles River	N/A
Mouse: male C57BL/6-Tg(TcraTcrb) 1100Mjb/J (OT-1)	own breeding	N/A

Oligonucleotides (5' -> 3')

Hk2 forward: TCAGAGCGCCTCAAGACAAG	Eurofins	N/A
Hk2 reverse: GTTGTCCAGTCCACGGTTCT	Eurofins	N/A
Cpt1a forward: CTCCGCTCGCTCATTCGG	Eurofins	N/A
Cpt1a reverse: GAGATCGATGCCATCAGGGG	Eurofins	N/A
Ldha forward: ATCGTGCCTAGCGGTCTCA	Eurofins	N/A

(Continued on next page)

Continued

REAGENT or RESOURCE	SOURCE	IDENTIFIER
Ldha reverse: CCATCATCTCGCCCTTGAGT	Eurofins	N/A
Atgl forward: GACAGCTCCACCAACATCCA	Eurofins	N/A
Atgl reverse: GCAAAGGGTTGGGTTGGTTC	Eurofins	N/A
Slc2a1 (Glut1) fw: CAGTTCGGCTATAACACTGGTG	Eurofins	N/A
Slc2a1 (Glut1) rev: GCCCCGACAGAGAAGATG	Eurofins	N/A
Lat1 forward: CCGGTCTTCCCCACTTGTC	Eurofins	N/A
Lat1 reverse: CTTGTCCTATGTCCTTCCCC	Eurofins	N/A
Snat1 forward: CCTTCACAAGTACCAGAGCAC	Eurofins	N/A
Snat1 reverse: GGCCAGCTCAAATAACGATGAT	Eurofins	N/A
Snat2 forward: GCCAACGAAGGAGGATCTTTATT	Eurofins	N/A
Snat2 reverse: GGTAGCTTGACATAGCCCCAA	Eurofins	N/A

Software and algorithms

Limma R package	Ritchie et al. (2015)	https://bioconductor.org/packages/release/bioc/html/limma.html
Shell script	N/A	http://crazyhottomm.blogspot.com/2018/02/convert-humangmt-file-to-mousefor-gsea.html
GSEA v3.0	Subramanian et al. (2005)	N/A
iTEM software package	Olympus	anlySISFive
FlowJo 10.8.0	BD Bioscience	www.flowjo.com
GraphPad Prism 9.2.0	GraphPad Software	www.graphpad.com/scientific-software/prism/

RESOURCE AVAILABILITY

Lead contact

Further information and requests for resources and reagents should be directed to and will be fulfilled by the Lead Contact, Percy Knolle (percy.knolle@tum.de).

Materials availability

No unique reagents have been developed in this study.

Data and code availability

All primary data from the experiments in this study are available upon reasonable request from the lead contact.

This paper does not report original code.

Any additional information required to reanalyze the data reported in this paper is available from the lead contact upon request

EXPERIMENTAL MODEL AND SUBJECT DETAILS

Wildtype male C57Bl/6 mice and OT1 CD8 T cell receptor (TCR) transgenic mice were held at specific-pathogen-free conditions according to the national guidelines of animal husbandry at the animal facility of the School of Medicine of the Technical University of Munich and experiments performed according to the permission by the Commission for Animal Safety of the State Council of Upper

Bavaria (55.2-2532.Vet_03-14-56). Mice were used at the age of 10 to 12 weeks for isolation of LSECs or splenic immune cells. The following monoclonal antibodies were used for cell phenotyping by flow cytometry: anti-CD146 (ME-9F1), anti-CD54 (3E2, BD Biosciences), anti-CD106 (CI429), anti-H2k^b (Rea932; Miltenyi Biotech, Germany), anti-MHC II (M5/114.15.2), anti-CD80 (16-10A1), anti-CD86 (GL1), anti-CD40 (3/23), anti-Ox40l (RM134L), anti-CD8 α (clone 53-6.7), anti-CD25 (PC61.5), anti-PD-1 (29F.1A12), anti-CD44 (IM7), CD62L (MEL-14), CD186 (CXCR6, SA051D1), CCR7 (4B12), CX3CR1 (SA011F11), CXCR3 (CXCR3-173), anti-KLRG1 (2F1), anti-FOXO1 (C29H4, Cell Signaling, #2880S), anti-IFN γ (XM61.2), anti-pFOXO1 (Ser256, Cell Signaling, #9461), anti-pAkt (SDRNR), anti-c-Myc (clone D84C12, Cell Signaling, #5605), anti-TNF (MP6-XT22), anti-granzyme B (anti-human, cross-reactive with mouse, Clone GB04), anti-Bcl-2 (100), anti-Ki67 (SolA15), anti-T-bet (eBio4B10), anti-EOMES (Dan11mag) (all from Biolegend or ThermoFisher Scientific). ELISA primary and secondary antibodies for detection of IL-2 and IL-6 in the cell culture supernatant were obtained from eBioscience (part of ThermoFisher Scientific, Waltham, USA). Mitotracker green and DiIC1(5) were obtained from InvitroGen (ThermoFisher); fluorescently labeled ovalbumin (Invitrogen, ThermoFisher Scientific, Waltham, USA) and acetylated low-density lipoprotein (acLDL) AF488 were obtained from Invitrogen, ThermoFisher Scientific, USA. Metabolic inhibitors (UK5099, BPTES and etomoxir) were purchased from Sigma Aldrich (part of Merck, Germany).

METHOD DETAILS

Isolation and culture of primary cell populations from liver and spleen

Murine liver sinusoidal endothelial cells (LSECs) were isolated from livers of C57Bl/6 mice using portal-vein perfusion, collagenase tissue digestion, density gradient centrifugation and immunomagnetic separation using anti-CD146 (Miltenyi Biotech, Germany). For some experiments mice received intravenous injection of ovalbumin (400 μ g/mouse) one hour before scarification and LSEC isolation. 1,6 x 10⁵ LSECs were then cultured on collagen-coated wells in growth medium (DMEM, Gibco, ThermoFisher Scientific, USA), 10 % FCS (Biochrome, Germany), 2 mM Glutamine (PanTMBiotech, Germany) at 37°C at ambient air oxygen levels and 10% CO₂ in a humidified incubator. At d2 after isolation, LSECs reached confluence and acquired a resting state. At this time point, CD146⁺ LSECs were fully functional showing highly potent scavenger activity and antigen-cross-presentation similar to their functional repertoire *in vivo*, as previously reported (Schurich et al., 2009). CD146⁺ LSECs that were devoid of contaminating CD11c⁺ dendritic cells were used for experiments at d2 after isolation. Murine DCs from spleen were isolated using mechanical disruption, 2 min lysis of erythrocytes with an ACK buffer and immuno-magnetic separation using anti-CD11c beads (Miltenyi Biotech, Germany). DCs were immediately processed for further experiments. All experiments were performed at 37°C and ambient air O₂ levels. Naive CD8⁺ T cells from OT-1 T cell receptor transgenic mice were isolated from spleen and immune-purified using a non-touch isolation strategy (Naive CD8⁺ isolation kit from Miltenyi Biotech, Germany) and cultured in RPMI 1640 medium containing FCS (10 %), L-glutamine (2 mM), Pen/Strep (100 U/ml), beta-mercaptoethanol (0,1 mM). For antigen-presentation assays, 1,6 x 10⁵ OT-1 CD8 T cells were added to LSECs, that were previously challenged with ovalbumin protein (200 μ g/ml) for 30 minutes, at a ratio of 1:1 for 18 hrs before analysis of T cell activation by determining IL-2 release into the cell culture supernatant by commercial ELISA. Co-culture of 1 x 10⁵ DCs with naive CD8 T cells at 1:1 ratio occurred in a U-shaped 96-well plate. Incubation of LSECs with oligomycin (1 μ M, Merck) or deoxyglucose (20 mM, Merck) was performed for 2hrs simultaneously with ovalbumin (200 μ g/ml, Merck, Darmstadt, Germany), followed by two washing steps before OT-1 CD8 T cells were added. Phenotypic and functional analysis by flow cytometry was performed as indicated after 24 or 72hrs of coculture in the presence of FOXO1 inhibitor AS1842856 (100 nM, Merck, #344355), anti-IL-6 (10 μ g/ml, clone MP5-20F3, BioLegend), anti-IL-2 (10 μ g/ml, clone S4B6, ThermoFisher Scientific) or anti-PD-L1 antibodies (10 μ g/ml, clone MIH5, ThermoFisher Scientific). Activation of LSECs, DCs or T cells was determined by measuring cytokine release into the supernatant using commercial antibodies for ELISAs for IL-6 or IL-2 (eBioscience, Thermo Fisher Scientific, Waltham, USA) following to the manufacturer's instructions.

Stimulation of CD8 T cells *in vitro*

Generation of CXCR6⁺ CD8 T cells from splenic CD8 T cells was performed as previously described (Dudek et al., 2021). In brief, 1 x 10⁶/ml splenic CD8 T-cells from C57Bl/6 mice were purified by immunomagnetic separation using AutoMACS (Miltenyi Biotec), were activated with plate-bound anti-CD3 (2 μ g/mL) for two days. Cells were removed and transferred to a new plate in the presence of TGF β (5 ng/mL, Peprotech, #100-21). After another two days, vital cells were isolated through Pancoll density centrifugation (1440 g, 20 min) and stimulated with IL-15R α /IL-15 (10 ng/mL, ThermoFisher, #14-8152-80) and TGF β for 24 hours to become highly enriched for CXCR6⁺, GzmB⁺ and CD69⁺ T cells.

Flow cytometry

Flow cytometric analyses were conducted on a spectral flow cytometer (SP6800, Sony Biotechnology, USA) and data obtained were analyzed using FlowJo software (Tree Star, USA). Fixable Viability Dye eFluorTM 780 (Thermo Fisher Scientific, USA) was used to exclude dead cells from analysis. Fluorochrome-labeled antibodies for cell phenotyping were purchased from BioLegend (USA) or ThermoFisher Scientific, if not specified otherwise.

For FOXO1 staining, cells were incubated with the unconjugated primary rabbit anti-mouse antibody overnight at 4°C followed by incubation with an AF488- (Cell Signaling, #4412s)- or AF647- (ThermoFisher Scientific, #A-21244)-conjugated secondary goat anti-rabbit antibody for one hour. For staining of phosphorylated proteins, cells were fixed and permeabilized in ice-cold methanol

(100%). Intracellular transcription factor staining for Bcl-2, Ki67, T-bet and EOMES was performed using the Foxp3/Transcription Factor Staining Buffer Set (ThermoFisher Scientific, #00-5523-00).

Mitochondrial mass and membrane potential were investigated by staining LSECs, DCs or CD8 T cells with mitotracker green (100 nM) and DilC1(5) (25 nM) diluted in PBS and incubated for 15 min at 37°C. Mitotracker green served as surrogate marker for mitochondrial mass and the potentiometric dye DilC1(5) to quantitatively determine mitochondrial membrane potential. The ratio of membrane potential per mitochondrial mass was calculated from mean fluorescence intensity of DilC1(5) and mean fluorescence intensity of mitotracker green for LSECs, DCs and CD8 T cells.

Glucose uptake by LSECs or CD8 T cells was performed by incubating cells for 15 min at 37°C in medium for uptake of deoxyglucose (100 μ M, 2-NBDG, ThermoFisher Scientific). Activation of mTOR pathway in LSECs was achieved using the mTOR agonist MHY1485 (1 μ M, Merck) and incubation for 1 h.

To measure scavenger activity, we added fluorescently labeled ovalbumin (20 μ g/ml, OVA-647, ThermoFisher Scientific, #O34784) or acetylated low-density lipoprotein (acLDL) (5 μ g/ml, ThermoFisher Scientific, #L23380) to LSECs for 30 min at 37°C before uptake was quantified by flow cytometry. Oligomycin and deoxyglucose (Sigma-Aldrich (Merck) were administered 10 min before fluorochrome-labeled ovalbumin or acLDL were added. Inhibitors against FOXO1 (100 nM) or NOTCH1 (10 μ M, DAPT, Tocris, #2634) were added 16 hours before incubation with fluorochrome-labeled ovalbumin. LSECs were gently detached with accutase (Merck) for flow cytometric analysis, which does not alter the expression levels of cell surface proteins, and incubated with anti-CD146 for 15 min, before a last washing step and analysis by flow cytometry.

Analysis of T cell effector functions

In order to determine the potential of T cells to produce the effector cytokines IFN γ and TNF, CD8 T cells after 72 hours of LSEC-priming were stimulated with PMA (5 ng/ml; Merck) and ionomycin (200 ng/ml, Merck) for 4 hours in the presence of Brefeldin A (1:1000, ThermoFisher Scientific) and Monensin (1:1000, ThermoFisher Scientific) and intracellular cytokines were stained by using the intracellular staining buffer set from ThermoFisher Scientific (USA). Staining of intracellular granzyme B (anti-human, cross-reactive with mouse, Clone GB04) was performed accordingly but without previous PMA/Ionomycin stimulation.

Proliferative capacity of LSEC-primed CD8 T cells (1×10^5 /well) treated with FOXO1 inhibitor that were restimulated with α anti-CD3/CD28 microbeads (Invitrogen) in the presence of recombinant mouse IL-12 (5 ng/ml, Peprotech) at 72 hours after priming was determined by calculating the fold change of cell numbers at day 0 and 3.

Antigen-specific cytotoxicity was evaluated *in vitro* by flow cytometry as previously described (Diehl et al., 2008). In brief, DC-primed and LSEC-primed CD8 T cells treated with FOXO1 inhibitor were cocultured for 4 hours with CFSE-labelled and SIIN-FEKL-loaded (10 μ M) splenocytes as target cells at several effector-to target ratios.

Determination of cellular bioenergetics

All measurements were performed using a Seahorse XF96 analyzer (Agilent Technologies, USA). LSECs were seeded directly after isolation on Seahorse cell culture plates (1.2×10^5 cells/well) and rested for 48hrs in growth medium prior to assay medium (XF-Base-Medium with 10 mM glucose (Agilent, Germany), 1 mM sodium-pyruvate and 2 mM glutamine (both Gibco, ThermoFisher Scientific, USA)). To address the metabolic profile of LSEC-primed CD8 T cells, CD8 T cells were carefully removed from the culture after 24 and 72 hours as LSECs firmly adhere to the plate to get highly pure CD8 T cells. To measure the oxidative profile, 2 μ M oligomycin, 1.5 μ M CCCP and 2 μ M antimycin A and rotenone (all Sigma Aldrich, Merck, Germany) each were injected during measurement of oxygen consumption and extracellular acidification. For glucose stress test, 10 mM glucose, 2 μ M oligomycin and 20 mM 2-deoxyglucose were consecutively injected into the ports. Analysis of long-chain fatty acid oxidation in LSEC-primed CD8 T cells was performed with XF Long Chain Fatty Acid Oxidation Stress Test Kit following the manufacturer's instructions (Agilent, #103672-100). LPS (100 ng/ml) was either directly injected or preincubated as described. Metabolic inhibitors were used at the following concentrations: UK5099 (inhibitor of the mitochondrial pyruvate carrier) at 2 μ M, BPTES (inhibitor of glutaminase) at 3 μ M and etomoxir (inhibitor of the carnitine palmitoyltransferase-1) at 4 μ M. DCs (1.5×10^5 cell/well) and LSEC-primed CD8 T cells (2×10^5 cell/well) were seeded in assay medium 2 hours before measurement. Bioenergetic profiles of LSEC-primed CD8 T cells were compared to memory CD8 T cells generated as described previously (van der Windt et al., 2012). In brief, immune-purified naïve OT-1 CD8 T cells were stimulated with plate-coated anti CD3 antibodies (5 μ g/ml, clone 145-2C11, Biolegend) in the presence of IL-2 (50 U/ml) for three days, followed by treatment with IL-15 (10 ng/ml, Peprotech, #200-15) for three days after removal of TCR stimulus. For glutamine and glucose-dependent measurements of OCR and ECAR in LSEC-primed CD8 T cells treated with FOXO1 inhibitor assay medium deprived of glutamine and glucose was used. Calculation of particular metabolic rates were performed as follows: basal oxygen consumption was calculated as the basal oxygen consumption rate (OCR) minus the residual rate after antimycin A/rotenone administration; ATP production was calculated as the difference between the OCR before and after oligomycin application; maximal respiration was calculated as difference between the maximal OCR, measured after CCCP injection, minus the residual OCR after antimycin A/rotenone; the spare respiratory capacity (SRC) was calculated as the difference between basal OCR at start of the measurement and the maximal rate after CCCP; basic glycolysis was calculated as the extracellular acidification rate (ECAR) at start of the measurements minus ECAR after injection of deoxyglucose; glycolytic reserve was calculated as the increase in ECAR after injection of oligomycin; and glycolytic capacity was calculated as the sum of basic glycolysis and glycolytic reserve. For normalization of results to cell numbers used in experiments, LSECs were counted after a 48 hrs resting period. Cells were stained with Hoechst dye (Invitrogen,

ThermoFisher Scientific, USA), fixed with 4% PFA and subjected to fluorescence microscopic measurement (Nikon Eclipse TE2000-S, Japan), cell nuclei were counted and total cell number per well were determined.

Transmission electron microscopy

Samples were fixed with 2.5% glutaraldehyde in 0.1M sodium cacodylate buffer, pH 7.4 (Electron Microscopy Sciences, USA) for 24 h at minimum. Thereafter glutaraldehyde was removed, and samples were washed three times with 0.1M sodium cacodylate buffer, pH 7.4. Post-fixation and prestaining was done for 45 to 60 min with 1% osmium tetroxide (Electron Microscopy Sciences, USA). Samples were washed three times with ddH₂O and dehydrated with an ascending ethanol series (15min with 30%, 50%, 70%, and 90% respectively and two times 10min with 100%). Subsequently, samples were embedded in Epon (Serva Electrophoresis GmbH, Germany). 60-70 nm thick ultrathin sections were cut at the Reichard-Jung Ultracut E microtome (Germany). Ultrathin sections were collected on formvar coated copper grids (Plano, Germany) and automatically stained with UranylLess EM Stain (Electron Microscopy Sciences, USA) and 3% lead citrate (Leica, Wetzlar, Germany) using the contrasting system Leica EM AC20 (Leica, Wetzlar, Germany). Imaging was carried out using the JEOL -1200 EXII transmission electron microscope (JEOL, Akishima) at 80 kV. Images were taken using a digital camera (KeenViewII; Olympus, Germany) and processed with iTEM software package (anlySISFive; Olympus, Germany).

Quantitative real-time PCR

RNA from LSEC-primed CD8 T cells was isolated according to the manufacturer's instructions (#T2010S, NEB). cDNA was generated using SensiFAST cDNA synthesis kit from Bioline (#BIO-65054). Primers against murine *Hk2*, *Ldha*, *Glut1*, *Cpt1a*, *Atgl*, *Lat1*, *Snat1* and *Snat2* were purchased from Eurofins (Munich) and the sequences are listed in the Supplementary Information. A mix of primer pairs, double distilled water and 2x Takyon Mix SYBR green assay (Eurogentec) was added to the cDNA and amplified copies were quantified by LightCycler 480 (Roche).

Geneset enrichment analysis (GSEA)

To execute geneset-enrichment analysis for FOXO1 and T_{rm} genesets in the micro-array dataset from Böttcher et al., 2013 (GSE27139), we downloaded the following gene sets from the molecular signature database (MsigDB): GSE46025_WT_VS_FOXO1/-_KLRG1_LOW_CD8_EFFECTOR_TCELL up and down gene sets. The T_{rm} related gene set was retrieved from Zhao et al. (Khan et al., 2019). DEGs were identified using Limma R package (Ritchie et al., 2015). To convert human gene sets into mouse orthologs, we used shell script (<http://crazyhottommy.blogspot.com/2018/02/convert-human-gmt-file-to-mouse-for-gsea.html>) and compared these mouse genes with our RNA-seq dataset. Gene set enrichment analyses of log2 fold changes from DEGs were performed using GSEA v3.0 (Subramanian et al., 2005). Fold changes along genesets were given as an input to the PreRanked tool from GSEA v3.0 which assessed the normalized enrichment score (NES). NES was considered significant based on false discovery rate (FDR) ($q \geq 0.25$).

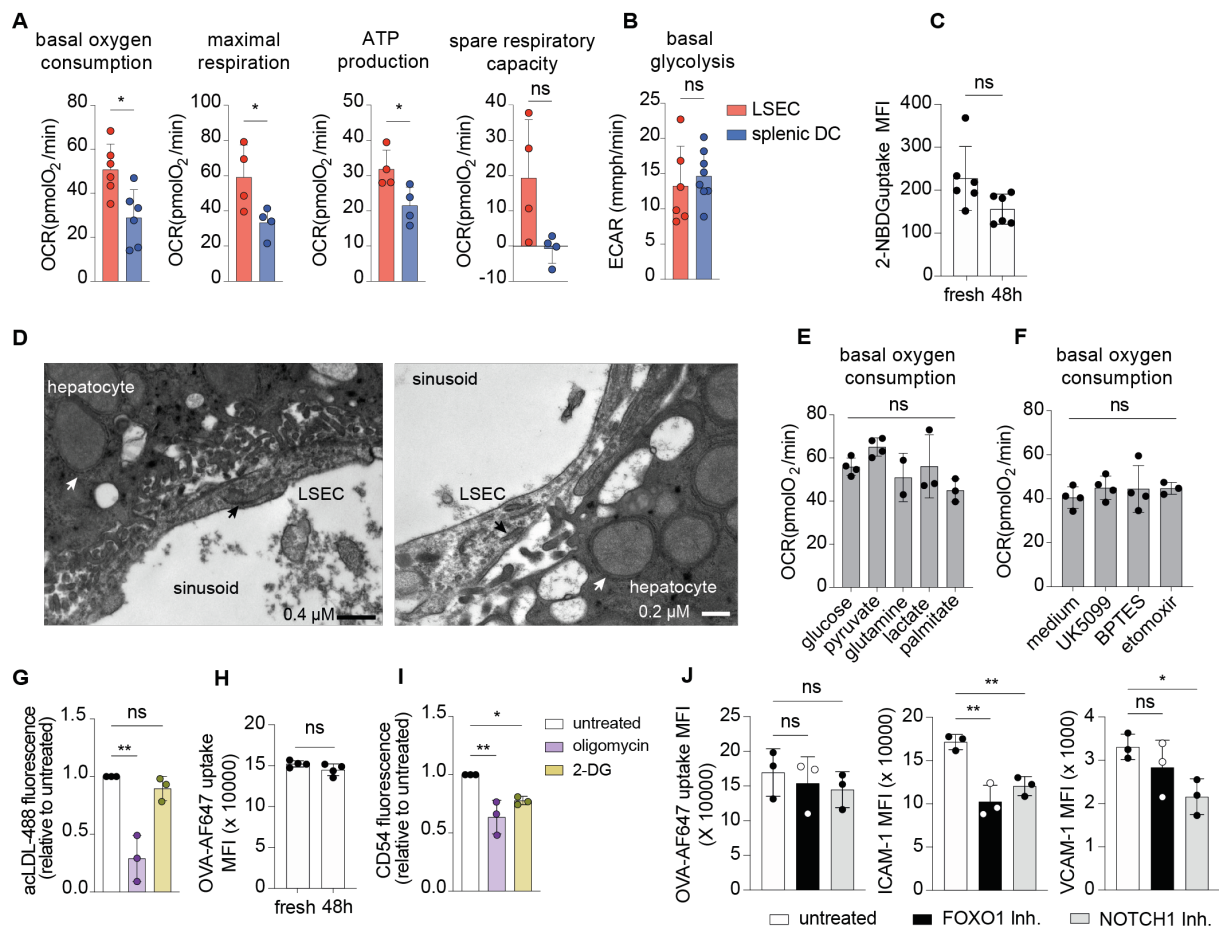
QUANTIFICATION AND STATISTICAL ANALYSIS

Results are represented as mean \pm standard deviation (SD). Statistical significance was accepted with $p < 0.05$. Statistical tests used for data analysis are specified in the figure legends. Briefly, comparison between two groups was tested with student's t-test. Three or more groups were compared using One-Way-ANOVA with Tukey's or Dunnett's posthoc-testing and grouped analyses were conducted using two-way-ANOVA and Tukey's, Dunnett's or Holm-Sidak posthoc testing. All statistics were performed with GraphPad Prism 6.0e, GraphPad Software, La Jolla California USA. Abbreviations denote: n.s. – not significant; * $p < 0.05$; ** $p < 0.01$; *** $p < 0.001$; **** $p < 0.0001$.

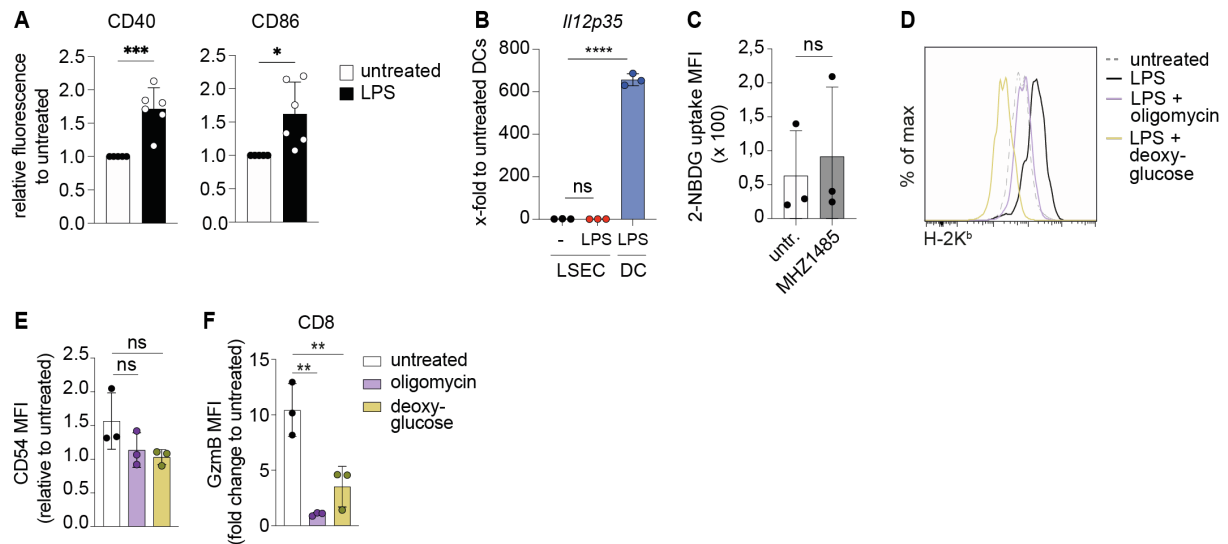
Supplemental information

**IL-6-induced FOXO1 activity determines
the dynamics of metabolism in CD8 T cells
cross-primed by liver sinusoidal endothelial cells**

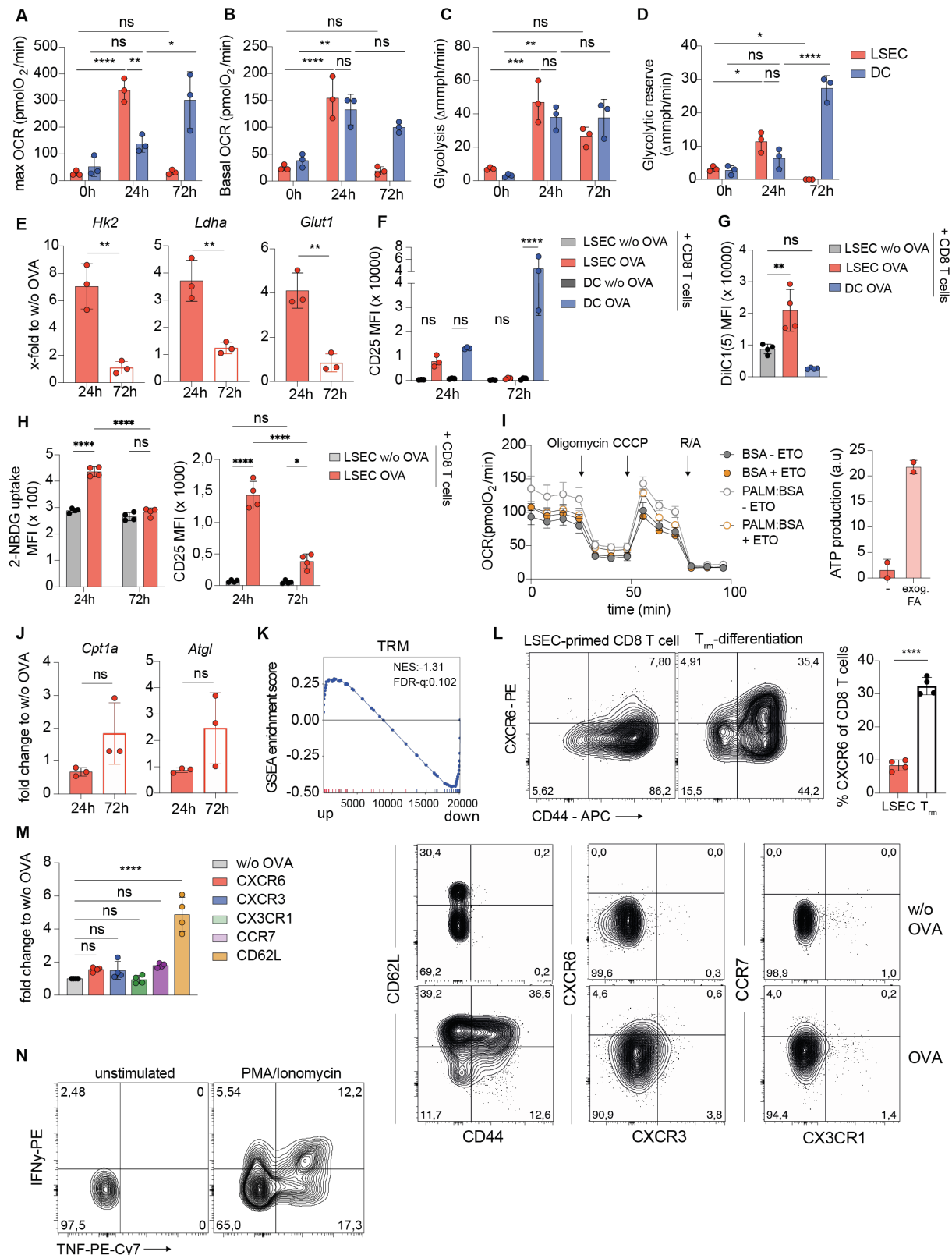
Michael Dudek, Kerstin Lohr, Sainitin Donakonda, Tobias Baumann, Max Lüdemann, Silke Hegenbarth, Lena Dübbel, Carola Eberhagen, Savvoula Michailidou, Abdallah Yassin, Marco Prinz, Bastian Popper, Stefan Rose-John, Hans Zischka, and Percy A. Knolle



Supplemental Figure 1: LSECs employ different energy substrates to fuel mitochondrial oxidative phosphorylation – related to Figure 1 (A,B) Values for basal oxygen consumption, maximal respiration, ATP production, spare respiratory capacity and basal glycolysis calculated from OCR and ECAR profiles ($n \geq 4$). **(C)** Flow cytometry analysis of 2-NBDG uptake in LSECs directly after isolation (fresh) or after 48 hours of cell culture to measure glucose uptake ($n = 6$). **(D)** Ultrastructural analysis of LSECs *in situ*, arrows depicting mitochondria in LSECs (black) and hepatocytes (white), scale bar 200 nm. **(E)** Basal OCR of LSECs after incubation with minimal medium devoid of nutrients supplemented with glucose, pyruvate, glutamine, lactate or palmitate ($n \geq 2$). **(F)** Basal OCR in LSECs after pharmacological inhibition of substrate-specific mitochondrial uptake pathways (UK5099 for pyruvate, BPTES for glutamine and etomoxir for long chain fatty acids) ($n = 4$). **(G,I)** Influence of deoxyglucose or oligomycin on LSEC scavenger activity of acetylated-LDL-488 (AcLDL-488) ($n = 3$) and on surface expression of CD54 determined by flow cytometric measurement ($n = 3$). **(H)** Flow cytometry analysis of OVA-AF647 uptake in LSECs directly after isolation (fresh) or after 48 hours of *in vitro* culture ($n = 4$). **(J)** Flow cytometry analysis of OVA-AF647 uptake in LSECs and surface expression levels of ICAM-1 and VCAM-1 at 12 hours after isolation in the presence of inhibitors that block transcriptional activity of the FOXO1 (100ng/ml, AS1842856) or the Notch1 signaling pathway (10μg/ml, DAPT). Data are representative of at least two separate experiments. NS, not significant. MFI, mean fluorescence intensity. OCR, oxygen consumption rate. ECAR, extracellular acidification rate One-way analysis of variance (ANOVA) with Dunnett's (E-G,I,J) multiple comparison test and unpaired two-tailed *t*-test (A-C,H). In A-C,D-J data are mean \pm s.e.m., errors are shown as s.d.

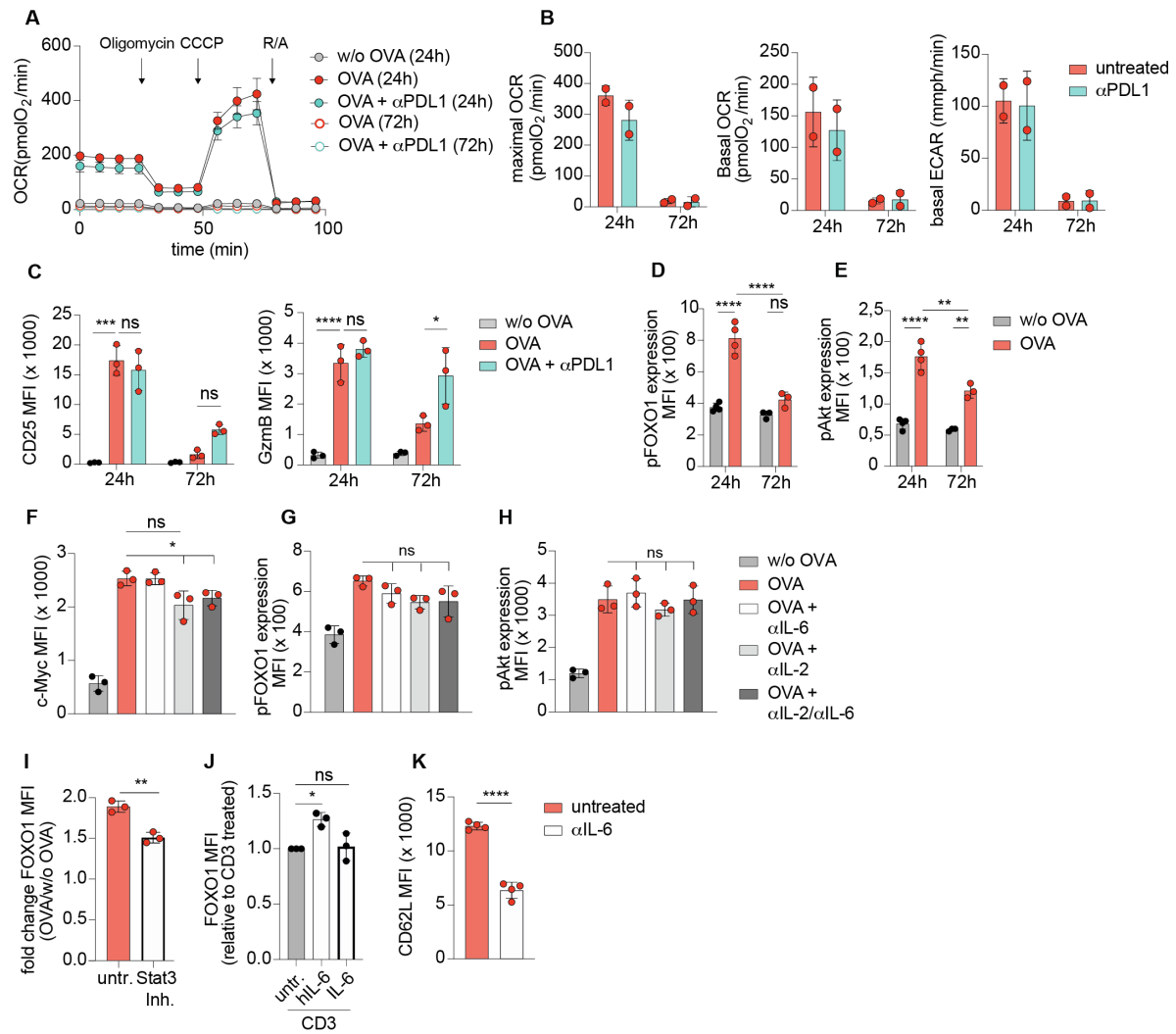


Supplemental Figure 2: Mitochondrial respiration and glycolysis are important for LSECs to efficiently prime CD8 T cells – related to Figure 2 (A) Flow cytometry analysis of surface expression levels of CD40 and CD86 on splenic CD11⁺ DC after LPS (100 ng/ml) stimulation for 24 hours ($n = 6$). (B) Gene expression level of *IL-12p35* in LSECs and splenic DCs treated with the TLR4-ligand LPS for 24 hours relative to untreated DCs and normalized to house-keeping gene *HPRT* ($n = 3$). (C) Glucose uptake by LSECs after mTOR agonist stimulation (MHY1485) ($n = 3$). (D,E) Histogram of H-2K^b expression (D) and quantification of CD54 expression (E) on LSECs after LPS challenge in absence or presence of deoxyglucose or oligomycin ($n = 3$). (F) GzmB expression in ovalbumin-specific H-2K^b-restricted CD8 T cells after activation by cross-presenting LSECs that were previously exposed to deoxyglucose or oligomycin ($n = 3$). Data are representative of at least two separate experiments. NS, not significant. MFI, mean fluorescence intensity. One-way analysis of variance (ANOVA) with Dunnett's (B,E,F) multiple comparison test and unpaired two-tailed *t*-test (A,C). In A-C,E,F data are mean \pm s.e.m., errors are shown as s.d.

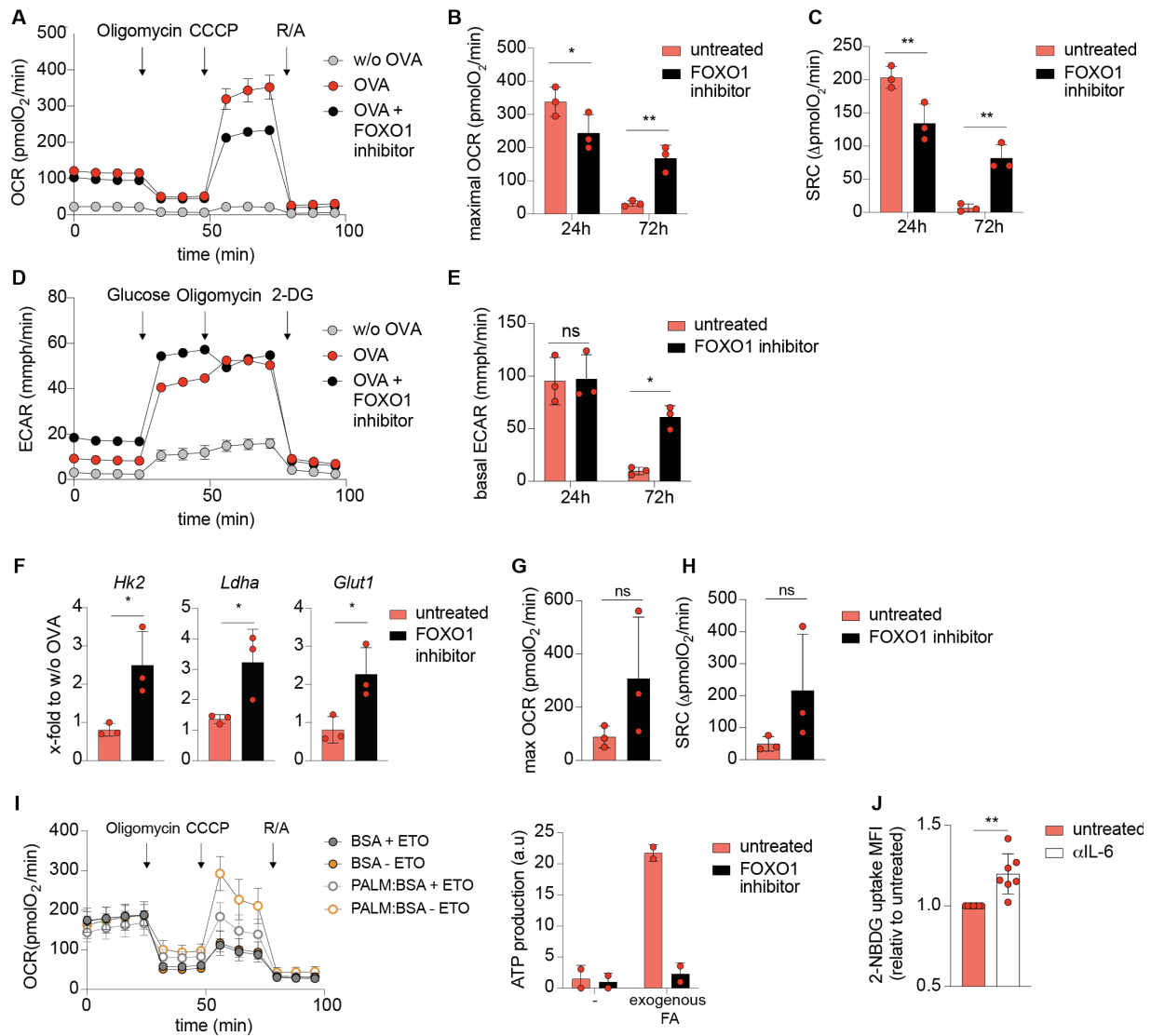


Supplemental Figure 3: Phenotype of LSEC and DC-primed CD8 T cells parallels metabolic dynamics in antigen-presenting cells – related to Figure 3. (A-D) Calculation of maximal respiration (A), spare respiratory capacity (B), glycolysis (C) and glycolytic reserve (D) from oxygen consumption rate (OCR) during mitochondrial stress test and extracellular acidification rate (ECAR) during glucose stress test measured by extracellular flux analysis in SIINFEKL-specific OT1 CD8 T cells after 24 and 72 hours of priming by LSECs and DCs ($n = 3$). (E) Gene expression levels of *Hk2*, *Ldha* and *Glut1* in LSEC-primed CD8 T cells after 24 and 72 hours of priming

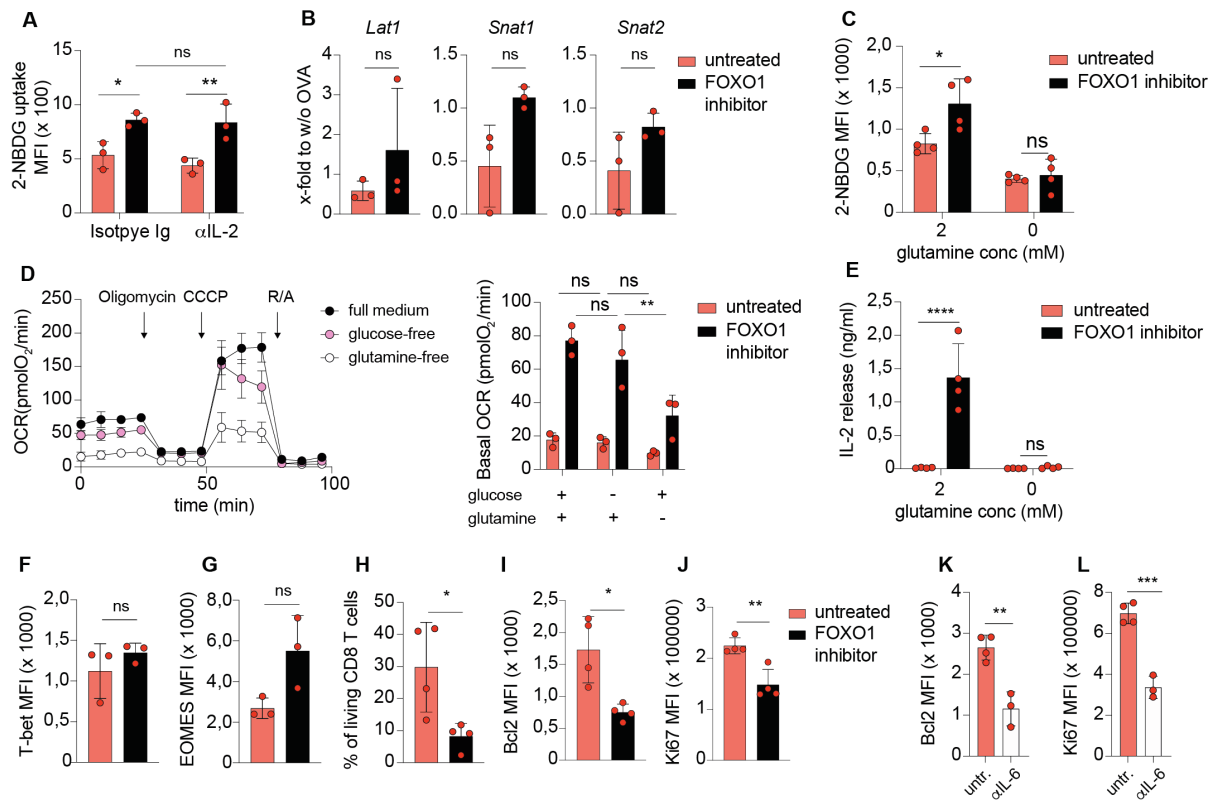
relative to SIINFEKL-specific OT1 CD8 T cells without stimulation (w/o OVA) normalized to house-keeping gene *18s* ($n = 3$). **(F)** Flow cytometry analysis of CD25 and CD44 expression of LSEC- and DC-primed CD8 T cells ($n = 3$). **(G,H)** One hour after mice received intravenous injection of ovalbumin (400 μ g/mouse) or PBS (w/o OVA), LSECs and splenic DCs were isolated and 16 hours later they were co-cultured with naïve OT-1 CD8 T cells for 24 and 72 hours. Flow cytometry analysis of DilC1(5), 2-NBDG uptake and CD25 expression in CD8 T cells ($n = 4$). **(I)** Representative metabolic flux profile of OCR in CD8 T cells at 72 hours after LSEC-priming. Fatty acid oxidation was determined by injections of palmitate (PALM), a free fatty acid conjugated to bovine serum albumin (BSA), and etomoxir, a CPT-1 inhibitor. ATP production of LSEC-primed CD8 T cells during FAO assay measured by metabolic flux analyzer ($n = 2$). **(J)** Relative gene expression levels of *Cpt1a* and *Atgl* in LSEC-primed CD8 T cells from **(E)** normalized to house-keeping gene *18s* ($n = 3$). **(K)** GSEA of differential expressed genes (DEG) of liver-primed CD8 T cells (Böttcher *et al.*, 2013) using gene set for liver residency (Zhao *et al.*, 2020). **(L)** Percentage of CXCR6⁺ T cells from CD8 T cells at 72 hours after LSEC-priming and from splenic CD8 T cells differentiated into T_{rm}-like CD8 T cells. **(M)** Flow cytometry analysis and dot plots of surface expression of CXCR6, CXCR3, CX3CR1, CCR7 and CD62L on LSEC-primed CD8 T cells after 72 hours of priming ($n = 4$). Fluorescence intensity is shown as fold change compared to naïve CD8 T cells that were cultured with LSECs which were not loaded with ovalbumin. **(N)** Expression of intracellular cytokines IFN γ and TNF in CD8 T cells after 72 hours of LSEC-priming restimulated for 4 hours with CD3/CD28 and IL-12 in the presence of the vesical transport inhibitor Brefeldin-A (BFA) and monensin. Data are representative of at least three separate experiments. NS, not significant. MFI, mean fluorescence intensity. NES, normalized enrichment score. FDR, false discovery rate. OCR, oxygen consumption rate. Two-way analysis of variance (ANOVA) with Tukey's **(A-D,F,H)** and One-way ANOVA with Dunnett's **(G,M)** multiple comparison test and unpaired two-tailed *t*-test **(I,K)**. In **A-D,F-J,L,M** data are mean \pm s.e.m., errors are shown as s.d.



Supplemental Figure 4. PD-1/PD-L1 signaling does not dampen the initial metabolic burst of LSEC-primed CD8 T cells – related to Figure 4. (A,B) Representative profile of OCR during mitochondrial stress test (A) measured by extracellular flux analysis in SIINFEKL-specific OT1 CD8 T cells after 24 and 72 hours of priming by LSECs treated with anti-PDL1 antibodies (10 µg/ml). Basal and maximal OCR and basal ECAR (B) were quantified after consecutive injections of several compounds ($n = 2$). (C) Flow cytometry analysis of CD25 and GzmB expression in LSEC-primed CD8 T cells from (A) ($n = 3$). (D-E) Phosphorylation levels of FOXO1 and Akt and c-Myc expression in SIINFEKL-specific OT1 CD8 T cells at 24 and 72 hours after cross-priming by LSECs ($n = 3-4$). (F-H) Phosphorylation levels of FOXO1 and Akt and c-Myc expression in LSEC-primed CD8 T cells treated with blocking antibodies against IL-6 (10 µg/ml) and IL-2 (10 µg/ml) at 24 hours after cross-priming ($n = 3$). (I) FOXO1 expression in LSEC-primed CD8 T cells at 24 hours after priming and treatment with Stat3 inhibitor S3I-201 (100 µM) ($n = 3$). (J) FOXO1 expression in splenic CD8 T cells stimulated with antibodies against CD3 (5 µg/ml) and treated with hyper IL-6 (10 ng/ml) and IL-6 (10 ng/ml) for 24 hours ($n = 3$). (K) CD62L expression on SIINFEKL-specific OT1 CD8 T cells after 72 hours of priming by LSECs and IL-6 inhibition ($n = 4$). Data are representative of at least two separate experiments. NS, not significant. MFI, mean fluorescence intensity. OCR, oxygen consumption rate. ECAR, extracellular acidification rate. Two-way analysis of variance (ANOVA) with Tukey's (C-E) multiple comparison test, one-way analysis of variance (ANOVA) with Tukey's (F-H) and Dunnett's (I) multiple comparison test and unpaired two-tailed t -test (I,K). In B-D data are mean \pm s.e.m., errors are shown as s.d.



Supplemental Figure 5. Increase in metabolism in LSEC-primed CD8 T cells after inhibition of FOXO1 activity at late time points – related to Figure 5. (A-E) Representative profiles of OCR (A) and ECAR during glucose stress test (D) measured by extracellular flux analysis in OT1 CD8 T cells at 24 hours after cross-priming by LSECs and treatment with FOXO1 Inhibitor AS1842856 (100 nM). Calculation of maximal respiration (B), spare respiratory capacity (C) and basal ECAR (E) ($n = 3$). (F) Gene expression levels of *Hk2*, *Ldha* and *Glut1* in LSEC-primed CD8 T cells at 72 hours after cross-priming and treatment with FOXO1 Inhibitor AS1842856 relative to untreated OT1 CD8 T cells without stimulation (w/o OVA) normalized to *18s* ($n = 3$). (G,H) Calculation of maximal respiration (G) and spare respiratory capacity (H) from *in vitro*-differentiated memory CD8 T cells at day 6 treated with FOXO1 Inhibitor AS1842856 (100 nM) for the last two days of culture ($n = 3$). (I) Representative metabolic flux profile and ATP production of LSEC-primed CD8 T cells treated with FOXO1 Inhibitor AS1842856 during FAO assay measured by metabolic flux analyzer ($n = 2$). (J) 2-NBDG uptake of SIINFEKL-specific CD8 T cells after 72 hours of priming by LSECs shown as fold change between CD8 T cells with IL-6 inhibition or not ($n = 7$). Data are representative of at least two separate experiments. NS, not significant. MFI, mean fluorescence intensity. OCR, oxygen consumption rate. ECAR, extracellular acidification rate. Two-way analysis of variance (ANOVA) with Tukey's (B,C,E) multiple comparison test and unpaired two-tailed *t*-test (F,H,J). In B,C,E,F,H,J data are mean \pm s.e.m., errors are shown as s.d.



Supplemental Figure 6: Deregulated metabolism in FOXO1-inhibited LSEC-primed CD8 T cells is glutamine-dependent – related to Figure 6. (A) Glucose uptake of LSEC-primed CD8 T cells treated with FOXO1 inhibitor at 72 hours after priming in the presence of neutralizing antibody against IL-2 or control immunoglobulin ($n = 3$). (B) Gene expression levels of glutamine transporters *Lat1*, *Snat1* and *Snat2* in LSEC-primed CD8 T cells at 72 hours after priming treated with FOXO1 Inhibitor AS1842856 relative to untreated SIINFEKL-specific OT1 CD8 T cells without stimulation (w/o OVA) and normalized to house-keeping gene *18s* ($n = 3$). (C) Flow cytometry analysis of glucose uptake with 2-NBDG in FOXO1-inhibited SIINFEKL-specific OT1 CD8 T cells after 72 hours of priming by LSECs cultured in glutamine-free medium ($n = 4$). (D) Representative metabolic flux profile of OCR during mitochondrial stress of FOXO1-inhibited LSEC-primed CD8 T cells at 72 hours after LSEC priming cultured in glutamine-or glucose-free medium and quantification of basal OCR ($n = 3$). (E) Determination of IL-2 release by ELISA from (C) ($n = 4$). (F,G) Fluorescence intensity of intracellular T-bet and EOMES detected by flow cytometry from LSEC-primed CD8 T cells at 72 hours after priming treated with FOXO1 Inhibitor AS1842856 (100 nM) ($n = 3$). (H) Flow cytometry analysis of the percentage of living FOXO1-inhibited LSEC-primed CD8 T cells 24 hours after restimulation with CD3/CD28 + IL-12 ($n = 4$). (I,J) Intracellular expression of Bcl2 and Ki67 in LSEC-primed CD8 T cells treated with FOXO1 Inhibitor AS1842856 (H,I) or with neutralizing antibodies against IL-6 (K,L) after restimulation with CD3/CD28 + IL-12 for 24 hours ($n = 4$). Data are representative of at least three separate experiments. NS, not significant. MFI, mean fluorescence intensity. OCR, oxygen consumption rate. Two-way analysis of variance (ANOVA) with Tukey's (A-E) multiple comparison test and unpaired two-tailed *t*-test (F-L). In A-L data are mean \pm s.e.m., errors are shown as s.d.